Mutant HTT seeding activity: a marker of disease progression and neurotoxicity in models of Huntington's disease

Anne Ast[1,8], Alexander Buntru[1,8], Franziska Schindler[1,8], Regine Hasenkopf[1], Aline Schulz[1], Lydia Brusendorf[1], Konrad Klockmeier[1], Gerlinde Grelle[1], Benjamin McMahon[1], Hannah Niederlechner[1], Isabelle Jansen[1], Lisa Maria Diez[1], Annett Boeddrich[1], Sophie A. Franklin[2], Barbara Baldo[3], Sigrid Schnoegl[1], Severine Kunz[4], Bettina Purfürst[4], Harm H. Kampinga[5], A. Jennifer Morton[6], Åsa Petersén[3], Janine Kirstein[7], Gillian P. Bates[2], Erich E. Wanker[1*]

[1] Neuroproteomics, Max Delbrueck Center for Molecular Medicine, 13125 Berlin, Germany and Berlin Institute of Health (BIH), 10178 Berlin, Germany

[2] Sobell Department of Motor Neuroscience, UCL Institute of Neurology, London WC1N 3BG, United Kingdom

[3] Translational Neuroendocrine Research Unit, Department of Experimental Medical Science, Lund University, Lund, Sweden

[4] Electron Microscopy Platform, Max Delbrueck Center for Molecular Medicine, Berlin, Germany

[5] Department of Cell Biology, University Medical Center Groningen, 9713 GZ Groningen, the Netherlands

[6] Department of Physiology, Development and Neuroscience, University of Cambridge, Cambridge CB2 3DY, United Kingdom

[7] Proteostasis in Aging and Disease, Leibniz-Institute for Molecular Pharmacology (FMP), Berlin, Germany

[8] Co-first author

* Correspondence: ewanker@mdc-berlin.de

SUMMARY

Self-propagating, amyloidogenic mutant huntingtin (HTT) aggregates may drive progression of Huntington's disease (HD). Here, we report the development of a FRET-based HTT aggregate seeding (FRASE) biosensor assay that enables the quantification of mutant HTT seeding activity (HSA) in complex biosamples from HD patients and disease models. Application of the FRASE assay revealed HSA in brain homogenates of presymptomatic HD transgenic and knock-in mice and its progressive increase with phenotypic changes, suggesting that HSA quantitatively tracks disease progression. Biochemical investigations of mouse brain homogenates demonstrated that HSA is high in fractions that contain small HTT fibrils but is low in fractions with large, insoluble HTT aggregates, indicating that small rather than large mutant HTT structures possess HSA. Finally, we assessed the neurotoxicity of mutant HTT seeds in an inducible *Drosophila* model transgenic for *HTT*. We found a strong correlation between HSA measured in adult neurons and the increased mortality of transgenic HD flies, indicating that FRASE assays detect disease-relevant, neurotoxic, mutant HTT structures with severe phenotypic consequences *in vivo*.

KEYWORDS

Huntington's disease, FRASE assay, HTT seeding, …

INTRODUCTION

Self-propagating protein aggregates are a pathological hallmark of a large number of neurodegenerative diseases including Huntington's disease (HD) (Jucker and Walker, 2013; Soto, 2012; Chiti et al., 2017). Recent studies indicate that aggregate pathology and associated tissue atrophy do not appear randomly throughout the brain but instead progress along distinct neuronal networks (Brundin et al., 2010; Goedert, 2015). Evidence was provided that amyloidogenic protein assemblies spread from cell to cell, converting free molecules of the same protein into aggregated species. This transcellular propagation may drive pathogenesis in neurodegenerative diseases (Guo and Lee, 2014; Meyer-Luehmann et al., 2006; Pecho-Vrieseling et al., 2014; Peelaerts et al., 2015). To understand the mechanisms of disease development and progression, it is of critical importance to specifically monitor the activity of self-propagating protein aggregates in complex biosamples.

A number of cell-free and cell-based assays have been established that allow the quantification of seeding activity of amyloidogenic aggregates in crude protein homogenates (Atarashi et al., 2007; Castilla et al., 2006; Holmes et al., 2014; Salvadores et al., 2014; Tan et al., 2015). These methods take advantage of the phenomenon that ordered protein aggregates are spontaneously formed from monomers by a nucleation-dependent process (Jarrett and Lansbury, 1993; Scherzinger et al., 1999), a relatively slow process *in vitro*. However, spontaneous amyloid formation can be accelerated by the addition of preformed aggregates that function as templates or seeds for the conversion of monomers from a soluble into an aggregated state (Cohen et al., 2012; Colby et al., 2007; Jarrett and Lansbury, 1993). Biosamples that contain seeding-competent protein aggregates might therefore stimulate the polymerization of soluble amyloidogenic proteins with related amino acid sequences in cell-free or cell-based seeding assays.

Based on this premise, the protein misfolding cyclic amplification (PMCA) technology and related cell-free methods (Atarashi et al., 2007; Atarashi et al., 2011; Saborio et al., 2001) have been developed, which allow the detection of minute quantities of seeding-competent PrP^{Sc} aggregates in various biomaterials prepared from patients or rodent models with prion disease (Castilla et al., 2005; Colby et al., 2007; Saa et al., 2006). Variants of the PMCA technology have also been applied for the amplification of amyloid-β, α-synuclein and HTT aggregates from biosamples (Du et al., 2011; Herva et al., 2014; Salvadores et al., 2014). A key feature of PMCA methods is that seed-mediated amyloid polymerization is indirectly monitored through the reporter dye Thioflavin T (ThT), which changes its fluorescence emission upon binding to ordered amyloid fibrils (Biancalana and Koide, 2010; LeVine, 1993). Also cell-based amyloid polymerization assays have been developed (Holmes et al., 2014; Tan et al., 2015). In these assays, ectopically expressed aggregation-prone reporter proteins with fluorescent tags such as ECFP or EYFP are generally utilized as biosensors for detecting amyloidogenic protein aggregates.

Recent studies with brain slices, cellular, fly and mouse models provide evidence that mutant HTT aggregates with pathogenic polyQ tracts indeed possess seeding activity and spread from cell to cell (Ren et al., 2009; Pecho-Vrieseling et al., 2014; Babcock and Ganetzky, 2015; Pearce et al., 2015), suggesting that proteopathic HTT seeding in HD patient brains or mouse models represents a causal process that drives pathogenesis (Brundin et al., 2010; Jeon et al., 2016). However, it currently remains unclear whether mutant HTT seeding is indeed responsible for dysfunction and neurodegeneration in disease. While several HTT aggregate species, i.e. small oligomers, protofibrils and large fibrillar structures, have been described as potentially pathogenic (Kim et al., 2016; Nucifora et al., 2012; Pieri et

al., 2012; Scherzinger et al., 1997), the HTT species that exhibit seeding activity *in vivo* still need to be pinpointed.

To be regarded as disease relevant, we propose that seeding-competent HTT aggregates need to be detectable in affected brain regions in patients and transgenic HD mouse models. To promote disease development, such structures should be present in model systems prior to the appearance of a disease phenotype. Also, their abundance in affected tissues should increase with the severity of disease symptoms. Finally, perturbation of mutant HTT seeding activity either through genetic manipulation or chemical compounds that target seeding-competent structures should influence the disease phenotype in model systems. In summary, to elucidate the potential importance of mutant HTT seeding in disease, it is crucial to (1) detect seeding-competent structures in relevant biosamples with high sensitivity and specificity, and (2) to investigate their potential impact on biological functions and phenotypes in well-characterized model systems.

Here, we describe the development of a **FR**ET-based HTT **a**ggregate **se**eding (FRASE) assay, which allows the quantification of mutant **H**TT **s**eeding **a**ctivity (HSA) in complex biosamples with high sensitivity and specificity. Application of the method revealed HSA in disease-affected brain tissues of HD patients and mouse models. Furthermore, we observed HSA in brain homogenates of presymptomatic HD mice and its progressive increase with disease development. Biochemical investigations of mouse brain homogenates revealed high HSA predominantly in soluble protein fractions that contain small, fibrillar HTT structures, suggesting that small rather than large HTT aggregates are responsible for this activity *in vivo*. Finally, using an inducible *Drosophila* model of HD, we demonstrated that the formation of small, seeding-competent HTTex1Q97 structures in adult neurons is associated with a

reduced lifespan of transgenic flies, indicating that FRASE assays detect neurotoxic structures. The potential implications of our results for the development of diagnostic tools and therapeutic strategies for HD and other polyglutamine diseases are discussed.

RESULTS

Establishment of a FRET-based HTT aggregate seeding assay with recombinant fibrillar Ex1Q48 aggregates

To monitor the seeding activity of mutant HTT aggregates in biosamples, we first developed a cell-free HTT aggregation assay with recombinant fluorescent reporter proteins (**Figure S1A)**. Two soluble glutathione S-transferase HTT exon-1 fusion proteins with 48 glutamines C-terminally fused to CyPet or YPet (GST-Ex1Q48-CyPet or -YPet) were produced in *E. coli* and purified to ~90% homogeneity using glutathione sepharose chromatography (**Figure S1B**).

Next, the recombinant proteins were cleaved with the sequence-specific PreScission protease (PSP) in order to release GST and to initiate the spontaneous aggregation of the fusion proteins Ex1Q48-CyPet and -YPet *in vitro*. The assembly of the tagged HTT exon-1 (HTTex1) proteins into insoluble aggregates over time was monitored using an established membrane filter retardation assay (FRA), which detects large HTTex1 aggregates but not monomers or small oligomers (Wanker et al., 1999; PMID: 29856013). We found that the fusion proteins Ex1Q48-CyPet and -YPet rapidly self-assemble into SDS-stable aggregates after a lag phase of 4-5 h (**Figure 1A**), indicating that the C-terminal fluorescent tags (**Figure S1A**) do not prevent the formation of stable, insoluble HTTex1 aggregates. Similar results were

obtained when the untagged fusion protein GST-Ex1Q48 (**Figure S1A**) was cleaved with PSP and the time-dependent formation of Ex1Q48 aggregates was monitored by FRA, confirming recently reported results (PMID: 29601786).

To investigate the morphology of spontaneously formed Ex1Q48-CyPet and -YPet aggregates, we analyzed the aggregation reactions with atomic force microscopy (AFM). After 24 h, we observed that the released CyPet- and YPet-tagged Ex1Q48 fusion proteins, similar to the untagged Ex1Q48 protein, form typical fibrillar protein aggregates (**Figure 1B**).

Next, we hypothesized that the aggregation of CyPet- and YPet-tagged HTTex1 fragments should lead to a time-dependent increase of FRET as the fluorescent tags are brought in close proximity when fibrillar aggregates are formed (**Figure 1C**). We treated mixtures of the GST-Ex1Q48-CyPet/-YPet fusion proteins (1:1 molar ratio; 1 – 3 µM concentrations) with PSP and quantified the spontaneous formation of Ex1Q48-CyPet/-YPet co-aggregates by repeated FRET measurements in a 384-well microtiter plate. We observed a time- and concentration-dependent increase of FRET efficiency (**Figure 1D**), confirming previous observations that amyloidogenic polyQ-containing HTTex1 fragments form stable co-aggregates in cell-free assays (Busch et al., 2003). In contrast, no time-dependent increase of FRET efficiency was observed in samples that were not treated with PSP (**Figure 1D**), underlining that the removal of the GST tag from the fusion proteins and the release of CyPet- and YPet-tagged Ex1Q48 fragments is critical for the self-assembly of co-aggregates. Proteolytic cleavage of the GST fusion proteins with PSP was confirmed by SDS-PAGE and immunoblotting (**Figure S1C**). AFM analysis confirmed that the samples indeed contain typical fibrillar HTTex1 co-aggregates (**Figure S1D**). Together, these experiments indicate that the time-dependent increase of FRET is

the result of the spontaneous formation of fibrillar Ex1Q48-CyPet/-YPet co-aggregates *in vitro* (**Figure 1C** and **S1D**).

In order to assess whether preformed fibrillar Ex1Q48 aggregates (**Figure 1B**), can seed the polymerization of the reporter fusion proteins Ex1Q48-CyPet/-YPet, we incubated a 1:1 mixture of the fusion proteins (1.2 µM total concentration) with PSP and different amounts of preformed Ex1Q48 fibrils as seeds and monitored the polymerization of the reporter proteins through quantification of FRET. We observed that addition of fibrils to aggregation reactions shortens the lag phase of Ex1Q48-CyPet/-YPet polymerization in a concentration-dependent manner (**Figure 1E** and **1F**), indicating that the added fibrillar HTTex1 aggregates possess seeding activity. We termed the established method, which permits the quantification of mutant **H**TT **s**eeding **a**ctivity (**HSA**) in samples of interest, **FR**ET-based HTT **a**ggregate **se**eding (**FRASE**) assay.

In independent control experiments, we also investigated whether a mixture of fusion proteins with polyQ tracts of a non-pathogenic length, GST-Ex1Q23-CyPet/-YPet (**Figure S1A**), can also be applied as reporter molecules to monitor HSA. We found that preformed, fibrillar Ex1Q48 seeds (**Figure 1B**) cannot induce FRET when they are added with PSP to GST-Ex1Q23-CyPet/-YPet reactions (**Figure S1E**), indicating that reporter molecules with pathogenic polyQ tracts are required to efficiently monitor HSA. Finally, we confirmed that addition of proteolytically cleaved GST-Ex1Q23 fusion protein as well as of uncleaved GST-Ex1Q23 or GST-Ex1Q48 fusion proteins do not shorten the lag phase of Ex1Q48-CyPet/-YPet polymerization (**Figure S1F**).

Both small fibrillar Ex1Q48 seeds and large bundles of fibrillar aggregates exhibit HSA in FRASE assays

Our initial experiments indicated that large bundles of preformed fibrillar Ex1Q48 aggregates (~1-2 μm in length; **Figure 1B**) can promote the polymerization of Ex1Q48-CyPet/-YPet fusions in FRASE assays (**Figure 1E** and **1F**). Next, we investigated whether small fibrillar Ex1Q48 structures, which can be obtained from large fibril bundles through sonication (Scherzinger et al., 1999), possess HSA. We sonicated preformed fibrillar Ex1Q48 aggregates (**Figure 1B**) for 1, 2, 5, 10, 30 and 60 seconds on ice and subsequently determined the seeding activities of the generated fractions using FRASE assays. We found that sonication reveals Ex1Q48 preparations with increased seeding activity (**Figure S2A** and **S2B**), indicating that besides large fibrillar aggregates also small Ex1Q48 structures, which increase in their abundance through sonication-induced fibril breakage (Cohen et al., 2013; Scherzinger et al., 1999), possess high seeding activity.

To confirm that smaller Ex1Q48 assemblies are produced through sonication, we compared the sonicated and non-sonicated samples using the FRA (Wanker et al., 1999). We found that the fibrillar Ex1Q48 aggregates in non-sonicated samples are efficiently retained on filter membranes (**Figure S2C**), while the HTTex1 structures in sonicated samples (>30s) are not.

Next, the sonicated and non-sonicated samples were analyzed using dot blot (DB) assays, which allow the identification of protein assemblies under native conditions on filter membranes independent of their size (Kayed et al., 2003). These experiments revealed Ex1Q48 immunoreactivity in both sonicated and non-sonicated samples (**Figure S2C**), confirming that sonication (>30s) leads to fibril breakage and the formation of small, soluble HTTex1 structures. Finally, we analyzed the generated

samples with AFM, confirming that sonication leads to the formation of small fibrillar Ex1Q48 structures (**Figure S2D**) and supporting the results obtained with denaturing FRAs (**Figure S2C**).

FRASE assays detect recombinant Ex1Q48 seeds with high sensitivity and specificity

To determine the sensitivity and the dynamic range of the FRASE assay, we first generated small Ex1Q48 seeds through sonication of preformed Ex1Q48 fibrils for 60 sec on ice. Analysis with blue native PAGE and immunoblotting confirmed that smaller Ex1Q48 structures with an average molecular weight of ~1,250 kDa (~90mers) were indeed produced through sonication (**Figure 2A**). As mentioned above, the non-sonicated fibrils (**Figure 1B**) were much larger in size and were retained in the pockets of blue native gels.

Next, a range of concentrations (0.001 – 1111.1 pM) of Ex1Q48 seeds were analyzed for their potency to stimulate Ex1Q48-CyPet/-YPet polymerization in FRASE assays. As expected, we observed a robust and dose-dependent shortening of the lag phase when sonicated Ex1Q48 structures were added to polymerization reactions (**Figure 2B** and **2C**). We determined a threshold of ~60 fM for detecting small Ex1Q48 seeds. We observed that FRASE assays respond quantitatively to the addition of sonicated Ex1Q48 seeds over a dynamic range of more than 4 orders of magnitude (**Figure 2B** and **2C**). At a concentration of ~560 fM the Z' factor, indicative of a robust assay when greater than 0.5 (Zhang et al., 1999), was 0.67 (**Figure 2C**).

Finally, we investigated the specificity of the FRASE assay for detecting HTTex1 aggregates. We produced fibrillar aggregates of the polypeptides α-

synuclein, tau, amyloid-β and IAPP *in vitro* and analyzed these structures for their potential to stimulate the polymerization of the reporter proteins Ex1Q48-CyPet/-YPet in FRASE assays. The unrelated fibrillar aggregates did not significantly diminish the lag phase of spontaneous Ex1Q48-CyPet/-YPet polymerization (**Figure 2D**), indicating that the FRASE assay specifically detects amyloidogenic HTTex1 aggregates. AFM analysis confirmed that fibrillar α-synuclein, tau, amyloid-β and IAPP aggregates were used (**Figure 2E**).

Mutant HTT seeding activity is detectable in brains of HD mice and patients

To investigate whether the FRASE assay enables the detection of mutant HSA in complex biosamples (**Figure 3A**), we first assessed crude brain homogenates prepared from 12-week-old R6/2Q212 transgenic mice (carrying ~212 CAGs) and age-matched controls. R6/2Q212 mice express low levels of the human HTTex1 protein with a very long polyQ tract and are a model for the aberrant HTT splicing that occurs in HD (Sathasivam et al., 2013). They show motor abnormalities from 8 weeks of age (Carter et al., 1999; Lione et al., 1999) and typical HTT inclusion bodies from 3-4 weeks onwards (Li et al., 1999), suggesting that brains of 12-week-old mice should contain HTT species displaying HSA. We detected high levels of HSA in crude brain homogenates of R6/2Q212 mice but not in those of age-matched littermate controls (**Figures 3B** and **3C**), indicating the presence of seeding-competent HTTex1 structures. Independent control experiments with the non-pathogenic reporter molecules Ex1Q23-CyPet/-YPet did not reveal detectable HSA in R6/2Q212 brain homogenates (**Figure S3A**), confirming our initial results (**Figure S1E**) that pathogenic polyQ tracts in reporter molecules are critical to efficiently monitor HSA.

Next, we assessed whether HSA is detectable in brain extracts of 12-week-old R6/2Q51 (Larson et al., 2015) mice, which express a mutant HTTex1 fragment with a polyQ tract of 51 glutamines (R6/2Q51). In comparison to R6/2Q212 mice, these mice do not yet have a disease phenotype at 12 weeks of age, suggesting that HSA should be lower. FRASE analysis revealed that brain homogenates of prodromal 12-week-old R6/2Q51 mice do not possess significant HSA (**Figure S3B**). However, activity was detectable in extracts of very old R6/2Q51 mice (104-105 weeks), which show signs of disease (unpublished data, AJM).

We next investigated whether HSA is detectable in the hypothalamus of mouse brains, in which the proteins HTT853-Q79 or HTT853-Q18 were overexpressed for 8 weeks using viral vectors. Previous studies have demonstrated that hypothalamic expression of HTT853-Q79 for 6 weeks leads to a dramatic gain of body weight and the formation of insoluble HTT protein aggregates (Hult et al., 2011). We found that HTT853-Q79 mice were significantly heavier than control and HTT853-Q18 mice (**Figure S3C**), confirming previous results (Baldo et al., 2013). We also observed a significantly higher HSA in brain homogenates of HTT853-Q79 compared to HTT853-Q18 mice and controls (**Figure S3D**), indicating that the abundance of seeding-competent mutant HTT conformers in specific mouse brain regions is associated with an increase in body weight.

We next examined whether HSA can be detected in affected brain regions of HD patients. Crude protein extracts prepared from cerebral cortex, caudate nucleus and cerebellum of postmortem patients and control individuals were systematically analyzed using the FRASE assay. Strikingly, HSA was invariably detected in HD but not in control samples (**Figure 3D**), indicating that the method is suitable to discriminate between patients and healthy individuals. Interestingly, HSA was

detectable in the cerebral cortex and the caudate nucleus, which contain neuronal inclusions and are severely affected in HD patients (Zuccato et al., 2010) while it was not observed in the cerebellum, which does not exhibit typical neuronal HTT inclusions (DiFiglia et al., 1997). Similarly, no HSA was detectable in postmortem brains of patients with Alzheimer's disease (AD) **(Figure S3E**) that typically contain fibrillar amyloid-β and tau aggregates (Goedert, 2015).

Finally, we were interested to clarify whether HSA in biosamples indeed originates from mutant HTT seeds. We produced brain extracts from symptomatic 12-week-old R6/2Q212 mice and littermate controls and immunodepleted potential mutant HTTex1 seeds using the monoclonal anti-HTT antibody MW8 (Ko et al., 2001), before systematic FRASE analysis. We observed a dramatic decrease of HSA in MW8-immunodepleted R6/2Q212 brain homogenates but not in homogenates treated with an isotype control antibody (**Figures S4A** and **S4B**), indicating that seeding-competent HTTex1 aggregates can be efficiently removed from R6/2Q212 mouse brain extracts by MW8 antibody treatment. As expected, we did not detect HSA in crude brain extracts of age-matched wild-type control mice (**Figures S4A** and **S4B**). SDS-PAGE and immunoblotting confirmed depletion of HTTex1 protein aggregates from brain homogenates by MW8 antibody treatment (**Figures S4C** and **S4D**).

FRASE assay detects mutant HSA in brains of presymptomatic HD transgenic and knock-in mice

To address whether seeding-competent mutant HTTex1 aggregates are detectable in brains of presymptomatic HD transgenic mice, we first analyzed non-

sonicated brain homogenates of young R6/2Q212 mice and age-matched controls using the FRASE assay. We detected significant HSA in brain extracts of 2-week-old R6/2Q212 mice (**Figure 3E**) that progressively increased over time. This result was also obtained with sonicated brain extracts (**Figure 3F**). With sonication, significant HSA was already detectable in brains of 1-day-old R6/2Q212 transgenic mice, indicating that seeding-competent HTTex1 structures are present in brains of R6/2Q212 mice long before inclusion bodies or motor abnormities can be detected (Davies et al., 1997; Zuccato et al., 2010).

Next, we investigated whether HSA is detectable in presymptomatic *Hdh*Q150 knock-in mice that express a full-length HTT protein with a pathogenic polyQ tract of ~150 glutamines (Lin et al., 2001). These mice develop symptoms much more slowly than R6/2Q212 mice (Mangiarini et al., 1996; Zuccato et al., 2010). They show onset of depressive-like symptoms by 12 months of age (Ciamei et al., 2015) and impairment of motor function at ~18 months of age. Widespread deposition of insoluble HTT aggregates throughout the brain is observed by ~22 months of age (Woodman et al., 2007). We systematically analyzed tissue homogenates prepared from cortex, striatum and hippocampus of 2-, 5- and 8-month-old heterozygous *Hdh*Q150 mice and littermate controls using the FRASE assay. We observed progressively increasing HSA in protein extracts from all three brain regions of *Hdh*Q150 but not from control mice (**Figure 3G**), confirming that mutant HTT seeds are detectable in HD mouse brains long before the appearance of neuronal inclusion bodies and motor abnormalities (Woodman et al., 2007).

HSA is detectable in soluble protein fractions after depletion of large, insoluble HTT aggregates by centrifugation

To investigate whether HSA in transgenic HD mouse brains originates predominantly from soluble or insoluble HTT aggregates, non-sonicated brain homogenates prepared from symptomatic 12-week-old R6/2Q212 mice were centrifuged for 20 min at 2,700 x g (low speed) or 18,000 x g (medium speed), respectively, and the resulting supernatant and pellet fractions ($S1_{Low}$, $P1_{Low}$ and $S1_{Med}$, $P1_{Med}$; **Figure 4A**) were analyzed with FRASE assays. Interestingly, HSA was high in the parental crude lysate and in the $S1_{Low}$ fraction, while it was relatively low in the $P1_{Low}$ fraction (**Figure 4B),** suggesting that it predominantly originates from soluble rather than insoluble HTTex1 aggregates. A similar result was obtained when the fractions $S1_{Med}$ and $P1_{Med}$ were analyzed (**Figure 4B**). However, after medium speed centrifugation HSA in the $P1_{Med}$ fraction was higher than in the $P1_{Low}$ fraction, indicating that mutant HTTex1 seeds can be removed from the brain homogenate using a higher centrifugation speed. This trend was even more pronounced when the generated $S1_{Med}$ fraction was subjected to a high-speed centrifugation (190,000 x g), resulting in the supernatant and pellet fractions S2 and P2 (**Figure 4A).** FRASE analysis revealed a significantly higher HSA in the P2 than in the S2 fraction, indicating that small seeding-competent HTTex1 aggregates can be removed from the soluble $S1_{Med}$ fraction by high speed centrifugation (**Figures 4A and B**).

To obtain a first hint about the size of the seeding-competent HTTex1 aggregates in the brains of R6/2Q212 mice, the supernatant and pellet fractions were analyzed using the established FRA (Wanker et al., 1999). We found HTTex1 immunoreactivity predominantly in the $P1_{Low}$ and $P1_{Med}$ fractions. In comparison, weak immunoreactivity was detected in the $S1_{Low}$ and no activity in the $S1_{Med}$, P2 and S2 fractions (**Figure 4C**), indicating that HSA in R6/2Q212 mouse brains predominately originates from small, soluble rather than from large insoluble HTTex1 protein assemblies.

Finally, we also assessed whether HTTex1 seeds are detectable in R6/2Q212 mouse brain extracts with transmission immunoelectron microscopy. Here, we focused on the pellet fraction P2 prepared by high speed centrifugation from the $S1_{Med}$ fraction (**Figure 4A**). It exhibits high HSA in FRASE assays but does not contain large, SDS-stable HTTex1 aggregates that are detectable by FRAs (**Figures 4B** and **4C**). We detected small, immunoreactive fibrillar HTTex1 assemblies with diameters of 10.2 ± 3.6 nm and lengths of 157.8 ± 64.1 nm in the P2 fraction, while such structures were not observed in the corresponding pellet fraction of control mice (**Figure 4D**). This suggests that very small, HTTex1 fibrils possess HSA in P2 fractions.

Establishment of an inducible HD *Drosophila* model for short-time expression of HTTex1 fragments in adult neurons

To elucidate whether HTTex1 seeds with pathogenic polyQ tracts are disease-relevant structures that cause dysfunction and toxicity in neurons, it is necessary to investigate their phenotypic consequences *in vivo* in the absence of large insoluble HTTex1 aggregates or the continuous overproduction of mutant disease protein. We hypothesized that the short-time production of small amounts of mutant HTTex1 seeds in adult neurons might lead to increased mortality of transgenic HD flies, even though mutant HTTex1 expression is reduced to a minimum.

To address this question, we generated two transgenic HD fly strains. Using the bacteriophage ΦC31 integration system, cDNAs encoding HTTex1 proteins with normal and pathogenic polyQ tracts (HTTex1Q17 and HTTex1Q97) were integrated into a predetermined intergenic locus (Bischof et al., 2007). The genotypes of the

newly created strains were confirmed by PCR using genomic DNA (**Figure S5A**). In order to investigate whether the two fly strains are comparable regarding their survival in the absence of HTTex1 expression, we generated w1118;HTTex1Q17 and w1118;HTTex1Q97 flies, which carry the transgenes but lack the GAL4 gene driver and therefore should not produce the HTTex1 proteins. Measuring the survival over time, we found that both fly strains showed a median life span of ~102 days (**Figure S5B**), indicating that the integration of transgenes does not influence fly survival.

To induce HTTex1 protein expression in adult neurons we used the elav GeneSwitch (elavGS) system, an inducible pan-neuronal driver (**Figures S5C**). The elavGS driver (Osterwalder et al., 2001) was applied previously to create adult-onset *Drosophila* models for spinocerebellar ataxia 7 (Latouche et al., 2007) and Alzheimer's disease (Sofola et al., 2010), suggesting that it may also be suitable to temporarily produce polyQ-containing HTTex1 proteins in neurons. Transgene expression in neurons of transgenic elavGS flies is induced when they are supplied with food containing the hormonal inducer RU486. Transgene expression can be switched off again, when flies are transferred back to food lacking the inducer (Rogers et al., 2012).

We first performed proof-of-principle experiments to investigate whether RU486 treatment induces transgene expression in elavGS;HTTex1Q97 flies. We incubated adult flies for 1, 3, 6 and 12 days on food containing RU486 (400 μM) and quantified HTTex1Q97 transcript levels in fly heads by qPCR. We measured high amounts of HTTex1Q97 transcripts in brains of RU486 treated but not untreated flies (**Figure S5D** and **S5E**), confirming the functionality of the RU486-inducible expression system. Similar results were obtained when elavGS;HTTex1Q17 flies were analyzed (data not shown).

Finally, we assessed whether in RU486 treated elavGS HD flies mutant HTTex1 aggregates and HSA can be detected in adult fly brains. Starting at an age of 3 days, we treated elavGS;HTTex1Q97 and elavGS;HTTex1Q17 flies for 24 days with the expression activating hormone RU486. Head lysates were prepared and subsequently analyzed by FRA and FRASE assays. We observed the formation of large SDS-stable HTTex1Q97 aggregates by FRA in head extracts of RU486 treated elavGS;HTTex1Q97 flies. However, such structures were not detected in untreated elavGS;HTTex1Q97 flies (**Figure S5F**). Similarly, no SDS-stable aggregates were detectable in RU486 treated and untreated elavGS;HTTex1Q17 and w1118;HTTex1Q17/Q97 control flies (**Figure S5F**), indicating that large, SDS-stable fibrillar HTTex1Q97 structures are only formed in fly neurons, when the expression of the mutant protein is induced by hormone treatment. Strikingly, in head lysates of hormone treated elavGS;HTTex1Q97 flies besides SDS-stable HTTex1Q97 aggregates (**Figure S5F)** also HSA was detectable with the FRASE assays (**Figure S5G),** indicating that seeding-competent fibrillar HTTex1 aggregates are formed in fly neurons. In contrast, HSA was undetectable in brains of untreated elavGS;HTTex1Q97 flies as well as in treated and untreated elavGS;HTTex1Q17 flies and in w1118;HTTex1Q17/Q97 control flies of the same age (**Figure S5G**).

Short-time expression of HTTex1Q97 in adult neurons decreases lifespan and locomotor activity of HD transgenic flies

We first assessed whether HTTex1 transcripts decline when elavGS;HTTex1Q97 flies are placed back on food without the inducer. We observed that HTTex1Q97 transcripts indeed rapidly decrease in neurons of untreated flies (within ~24 h; **Figures S6A** and **S6B**), confirming previously published results that

transgene expression can be efficiently turned off in transgenic elavGS flies (Rogers et al., 2012).

We next investigated whether both long- and short-time expression of HTTex1Q17 or HTTex1Q97 in adult neurons influences survival of HD transgenic flies. Starting at an age of 3 days, we treated elavGS;HTTex1Q17 and GS;HTTex1Q97 flies either continuously or only for a short time of 3 or 6 days with the expression activating hormone RU486 (**Figure 5A**); survival was measured over time by counting dead flies. We found that the lifespan of chronically RU486 treated elavGS;HTTex1Q97 flies was significantly reduced in comparison to untreated flies (**Figure 5B** and **5C**). In strong contrast, chronic treatment with RU486 did not shorten the lifespan of elavGS;HTTex1Q17 flies, indicating that the neuronal expression of HTTex1Q97 but not of HTTex1Q17 promotes mortality. We calculated a median lifespan of ~30 and ~85 days for treated and untreated elavGS;HTTex1Q97 flies, respectively, indicating that chronic RU486 exposure shortens median lifespan by ~65%. Interestingly, short-time RU486 treatment also dramatically shortened the lifespan of elavGS;HTTex1Q97 flies. We calculated median lifespans for 3- and 6-day-treated flies of ~38 and ~33 days, respectively (**Figure 5B** and **5C**), indicating that survival of both short- and long-time RU486 treated elavGS;HTTex1Q97 flies is similar.

As a behavioral measure of neuronal dysfunction, locomotor activity was assessed in our inducible HD model using a negative geotaxis (climbing) assay that has been extensively applied to characterize fly models of neurodegenerative diseases (Latouche et al., 2007; Sofola et al., 2010). We observed that RU486-treated, elavGS;HTTex1Q97 flies show a significant decline in climbing behavior in comparison to untreated controls (**Figure 5D**), confirming that both short and long-

time expression of HTTex1Q97 in adult neurons induces dysfunction and neurotoxicity with severe phenotypic consequences.

Formation of small, seeding-competent HTTex1Q97 structures in adult neurons correlates with reduced survival of HD transgenic flies

We first assessed whether reduced survival of long- and short-time RU486-treated elavGS;HTTex1Q97 flies (**Figure 5B and 5C**) is associated with increased deposition of large, SDS-stable HTTex1 aggregates in neurons, which can be quantified by FRAs (Wanker et al., 1999). Head lysates were prepared from continuously and short-time (3 and 6 days) RU486-treated and untreated flies (**Figure S6C**) and subsequently analyzed by FRA using the anti-HTT antibody MW8 (Ko et al., 2001). We found that the abundance of large, SDS-stable HTTex1Q97 aggregates was much higher in heads of chronically RU486-treated elavGS;HTTex1Q97 flies than in heads of short-time-treated flies (**Figure 5E**), indicating that the formation of large, SDS-stable HTTex1Q97 aggregates in neurons cannot explain the observed mortality of HD transgenic flies, which is similar for short- and long-time RU486-treated flies (**Figure 5C**). A similar result was obtained when the formation of large HTTex1Q97 aggregates in fly heads was quantified by FRAs using the anti-HTT antibody MB5492 (**Figure S6D**). Together these experiments indicate that the accumulation of large, SDS-stable HTTex1Q97 aggregates in neurons does not correlate with the observed mortality of short- and long-time RU486-treated elavGS;HTTex1Q97 flies (**Figure 5B**).

Next, we also investigated the formation mutant HTTex1 aggregates in brains of hormone treated and untreated elavGS;HTTex1Q97 flies using an

immunohistochemical method. We dissected whole brains of 27 day-old short and long-time treated elavGS;HTTex1Q97 flies (**Figure S6C**) and incubated them with the monoclonal anti-HTT antibody MAB5492. As a control, the brain sections were also immunoassayed with an anti-RBP (RIM-binding protein) antibody, which detects synapses in fly brains (LIT). As expected, we detected high amounts of HTTex1Q97 aggregates (green puncta) in long-time and lower amounts in short-time (3 and 6 days) hormone-treated HD flies (**Figure S6E**), confirming the results obtained with FRAs (**Figure 5E**). Interestingly, our immunohistochemical investigations also revealed that very low amounts HTTex1Q97 aggregates are detectable in 27 day-old non-induced elavGS;HTTex1Q97 flies (**Figure S6E**), indicating low levels of mutant HTTex1 protein are also expressed in the absence of hormone treatment. However, this low level expression of HTTex1Q97 was not sufficient to significantly shorten the lifespan of HD transgenic flies (**Figure 5C**).

Finally, we used the FRASE assay to quantify HSA in head lysates prepared from long- and short-time RU486-treated elavGS;HTTex1Q97 flies to determine whether seeding activity better predicts the survival phenotype than the detection of large aggregates with FRAs (**Figure 5E**). Strikingly, we measured high HSA in head lysates of both short- and long-time RU486-treated flies (**Figure 5F** and **5G**), demonstrating that the FRASE assay provides information that is fundamentally different from that obtained with FRA. As seeding activity in neurons of short-time treated flies cannot result from large fibrillar aggregates (**Figure 5E** and **S6D**), it must be due to smaller structures that are not retained by the filter membrane. In comparison to RU486-treated elavGS;HTTex1Q97 flies, HSA was undetectable in head lysates of elav;HTTex1Q17 control flies (**Figure 5F)**.

In contrast to the FRA results (**Figure 5E** and **S6D**), HSA levels measured with the FRASE assay (**Figure 5F** and **5G**) correlate significantly better with the increased mortality of RU486-treated elavGS;HTTex1Q97 flies (**Figure 5H**). Together, these experiments suggest that the formation of small seeding-competent HTTex1Q97 structures is necessary and sufficient to trigger dysfunction and neurotoxicity in neurons of elavGS;HTTex1Q97 flies.

Short-time expression of the molecular chaperone Hsp70 in adult neurons extends the lifespan of HD transgenic flies

Previous studies have demonstrated that the human molecular chaperone Hsp70 (*HSPA1L*) can reduce polyQ-mediated dysfunction and neurodegeneration in *Drosophila* models (LIT, LIT), suggesting that it may also influence HSA and toxicity in neurons of adult HTTex1Q97 transgenic flies. To address this question, we generated elavGS;HSPA1L;HTTex1Q97 flies, which facilitate the short-time co-production of both Hsp70 and HTTex1Q97 in adult neurons upon hormone treatment. We first assessed whether RU-486 treatment induces similar levels of HTTex1Q97 transcripts in brains of elavGS;HSPA1L;HTTex1Q97 and elavGS;HTTex1Q97 HD control flies. We treated 3-day-old flies for 6 days with RU-486 (400 μM) and subsequently quantified mutant HTTex1 transcript levels in fly heads by qPCR. We confirmed that hormone treatment stimulates HTTex1Q97 expression in neurons (**Figure S7A**). Furthermore, we observed that in both strains HTTex1Q97 transcript levels are very similar, indicating that co-expression of *HSPA1L* does not significantly influence HTTex1 expression in elavGS;HSPA1L;HTTex1Q97 flies.

To confirm the expression of Hsp70 in elavGS;HSPA1L;HTTex1Q97 flies, we next also analyzed protein extracts from heads of hormone treated animals by SDS-PAGE and immunoblotting. As expected, in head lysates prepared of hormone-treated flies a relatively high concentration of Hsp70 protein was detectable (**Figure S7B**), confirming that transgene expression is induced in HD flies. Furthermore, we observed similar Hsp70 levels in brains of hormone-treated elavGS;HSPA1L;HTTex1Q97 and elavGS;HSPA1L flies (**Figure S7B**), indicating that HTTex1Q97 co-expression (**Figure S7A)** does not significantly influence Hsp70 protein production in neurons of transgenic elavGS;HSPA1L;HTTex1Q97 flies.

Finally, we assessed whether short-time expression of Hsp70 (for 6 days) in adult neurons of 3-day-old elavGS;HSPA1L;HTTex1Q97 HD flies is sufficient to alter their survival phenotype. In control experiments, the short-time expression of HTTex1Q97 alone in elavGS;HTTex1Q97 flies was also investigated. Strikingly, we found that RU-486 treated elavGS;HSPA1L;HTTex1Q97 flies have a median lifespan of ~39 days, while it was ~33 days for hormone-treated elavGS;HTTex1Q97 flies (**Figure 6A-6C**). This indicates that even short-time co-expression of Hsp70 in adult neurons is sufficient to improve the survival of elavGS;HSPA1L;HTTex1Q97 flies. As expected from our initial studies (**Figure 5B**) a median lifespan of ~85 days was observed for non-treated elavGS;HTTex1Q97 flies.

Co-expression of Hsp70 decreases the abundance large HTTex1Q97 aggregates and of HSA in neurons of HD transgenic flies

To examine whether short-time expression (6 days) of Hsp70 in adult neurons influences mutant HTTex1 aggregation, head lysates of 13-day-old RU-486-treated

elavGS;HSPA1L;HTTex1Q97 flies were analyzed by FRAs. We found that in comparison to hormone treated elavGS;HTTex1Q97 control flies, the abundance of large, SDS-stable HTTex1Q97 aggregates was significantly decreased in neurons of elavGS;HSPA1L;HTTex1Q97 flies (**Figure 6D**), supporting previous observations that high levels of Hsp70 proteins can decrease the formation of large HTTex1 aggregates (LIT, LIT). Strikingly, in head lysates of RU-486-treated elavGS;HSPA1L;HTTex1Q97 flies in comparison to elavGS;HTTex1Q97 control flies HSA detected by FRASE assays was also significantly decreased (**Figure 6E and 6F**), substantiating our hypotheses that seeding-competent HTTex1Q97 aggregates cause toxicity and dysfunction in fly neurons.

Finally, we addressed the question whether the molecular chaperone Hsp70 associates with mutant HTTex1 aggregates in fly neurons. Immunohistochmical investigations of brain slices prepared from 9 day-old elavGS;HSPA1L;HTTex1Q97 flies treated for 6 days with the hormone Ru-486 revealed co-localization of the molecular chaperone Hsp70 and HTTex1Q97 aggregates in HD brains (**Figure 6G**), supporting previous observations that Hsp70 directly interacts with mutant polyQ-containing HTTex1 proteins and decreases their aggregation propensities (LIT, LIT).

Depletion of Hsc70 increases both toxicity and Q35-YFP seeding activity in a *C.elegans* model

Our studies indicate that short-time overproduction of the molecular chaperone Hsp70 improves survival of elavGS;HSPA1L;HTTex1Q97 HD flies and decreases HSA in neurons (**Figure 6C** and **6F**), suggesting that a decrease of chaperone expression might have the opposite effects on seeding and mHTT-induced toxicity in

model systems. To address this question, we performed RNAi knockdown experiments in transgenic worms that overproduce the aggregation-prone protein Q35-YFP in wall muscle cells. Previous studies have demonstrated that Q35-YFP aggregation in muscle cells leads to motor impairment and that this phenotype gets even more severe when the expression of the *hsp-1* gene *(*encoding the molecular chaperone Hsc70) is knocked down by RNAi (Brehme et al., 2014; Nollen et al., 2004). We treated Q35-YFP expressing worms with hsp-1 RNAi and assessed their movement at day 5 of adulthood. We observed a significant reduction of motility in RNAi-treated in comparison to untreated worms (**Figure S8A**), confirming previously published results (Brehme et al., 2014). Furthermore, this phenotypic change was associated with a significant increase in Q35-YFP seeding activity in FRASE assays (**Figure S8B** and **S8C**), supporting our hypothesis that HSA is maker of dysfunction and toxicity in model systems.

DISCUSSION

There is increasing experimental evidence that self-propagating mutant HTT aggregates, or seeds, play an important role in the development of disease in HD model organisms (Babcock and Ganetzky, 2015; Brundin et al., 2010; Pecho-Vrieseling et al., 2014). Whether they are indeed critical or even responsible for the appearance and progression of disease, however, is still unclear. To address this question, we developed a FRET-based biosensor (FRASE) assay that enables the sensitive quantification of mutant HTT seeding activity (HSA) in complex biosamples. With this assay in hand, we assessed the potential correlation between HSA in affected tissues and the appearance of disease phenotypes in HD transgenic mice (**Figures 3**). We detected robust HSA in crude brain extracts of mice weeks before

manifestation of disease (**Figures 3E-3G**). Furthermore, we observed an increase of mutant HSA in mouse brain extracts concomitantly with the appearance of symptoms, suggesting that it quantitatively tracks disease progression. Finally, comprehensive mechanistic studies with a newly established inducible *Drosophila* model of HD indicate that the formation of small, seeding-competent HTTex1Q97 structures in adult neurons are necessary and sufficient to significantly shorten the lifespan of HD flies, supporting our hypothesis that mutant HTT seeding is a disease-relevant process causing dysfunction and neurotoxicity. Taken together, these studies indicate that HSA is a valuable early disease marker that can predict severe downstream phenotypic changes in various HD models.

The fluorescent dye Thioflavin T (ThT) is currently utilized in a large number of cell-free assays as a reporter molecule to monitor the seeding activity of amyloidogenic protein aggregates (Gupta et al., 2012; Salvadores et al., 2014). ThT exhibits enhanced fluorescence when it is bound to β-sheet-rich amyloid structures (LeVine, 1993). However, its binding to such structures is significantly decreased, when competing proteins are present in complex amyloid polymerization reactions (Biancalana and Koide, 2010; LeVine, 1993). Therefore, previously established ThT-based seeding assays are relatively insensitive when complex biosamples such as brain homogenates are analyzed: For example, it was demonstrated that mutant HTT seeds need to be enriched from crude mouse brain homogenates in order to be successfully amplified with a ThT-based HTT seeding assay (Gupta et al., 2012).

To overcome these limitations, we have established a FRET-based biosensor assay, which does not require ThT reporter molecules for the quantification of HSA in biosamples. Two fluorescently tagged aggregation-prone HTT exon-1 fusion proteins with 48 glutamines (Ex1Q48-CyPet/-YPet) are used as reporter molecules to monitor

seeding activity (**Figure 1C**). These proteins self-assemble into stable fibrillar co-aggregates under both seeded and non-seeded conditions and yield FRET-based aggregation profiles from which HSA in biosamples is quantified (**Figure 3A**). This process is highly robust and affected by contaminating proteins in complex biosamples only to a very small extent. Therefore, the FRASE assay can be employed without the need for upstream purification of HTT seeds, which would complicate the protocol and decrease accuracy of quantification. Also, the method is highly sensitive and specific (**Figure 2B-2E**), indicating that it is a suitable tool for routine application in research and development.

We observed high HSA in soluble fractions of transgenic HD mouse brain extracts (**Figure 4B** and **4C**), suggesting that greater seeding activity is associated with smaller particles. However, inclusions with insoluble fibrillar HTTex1 aggregates (Bäuerlein et al., 2017) may also possess seeding activity. Further studies will be necessary to purify fibrillar HTTex1 structures of different sizes from mouse and fly brains and to compare their specific seeding activity (i.e., seeding activity per unit of protein). We assume that there is a continuum of mutant HTT species in disease brains that all have some seeding activity. However, similar to previously published results for infectious prion species (Silveira et al., 2005), we provide initial evidence that the specific activity may be higher for smaller mutant HTTex1 structures than for larger aggregates.

Our results are in agreement with previous investigations indicating that small, fibrillar polyQ-containing HTT assemblies are detectable in the cytoplasm of cells besides large inclusions with fibrillar mHTT aggregates (Sahl et al., 2012; Sathasivam et al., 2010). They are also consistent with experimental studies demonstrating that proteotoxicity in mammalian cells is associated with small,

diffusible HTT oligomers rather than large inclusions (Arrasate et al., 2004; Kim et al., 2016; Leitman et al., 2013; Taylor et al., 2003). However, our present study advances beyond the state-of-the-art. For the first time, we provide experimental evidence that seeding of HTTex1Q97 is associated with dysfunction and neurotoxicity in neurons of HD transgenic flies in the absence of detectable large, insoluble HTT aggregates (**Figures 5 and 6**). We suggest that small, seeding-competent structures are formed which shorten the lifespan of HD flies through aberrant interaction with essential fly proteins, perturbing their normal physiological functions. Further mechanistic investigations, however, will be necessary to elucidate the critical downstream molecular changes that are induced by HTTex1Q97 seeding in neurons of HD transgenic flies.

Together, our investigations indicate that mutant HTT seeds in brains of HD transgenic mice and flies are an early pathological manifestation of disease; they increase in their abundance with the development of disease phenotypes (**Figure 3E-3G**). We suggest that HSA in mouse brain extracts is a biological marker of disease long before onset. Previous studies argue that the abundance of large insoluble HTT aggregates in brains of HD mice and patients is not predictive for the development of symptoms (Kuemmerle et al., 1999; Slow et al., 2005). However, neuronal inclusions with insoluble aggregates are commonly detected with immunohistological methods, which fail to identify small, seeding-competent HTT assemblies in disease brains. The application of the FRASE assay overcomes this important limitation associated with standard histology and is likely to yield new mechanistic insights into the progressive development of HD.

We propose that in future drug trials with transgenic HD mice HSA could be utilized as an outcome marker to monitor the efficacy of therapeutic molecules *in*

vivo, before and independent of changes in phenotype. We detected robust HSA in the striatum of 2-month-old HdhQ150 transgenic mice (**Figure 3G**). Drug treatment could start before that point in time and animals could be assessed for HSA at any age after two months. Furthermore, we propose that the FRASE method can be applied as a drug screening assay to identify therapeutic molecules that directly target mutant HTT seeding *in vitro*. Because the assay can monitor mutant HSA in protein extracts from postmortem patient brain and transgenic animals (**Figure 3D-3G**), it seems now feasible to investigate therapeutic candidate molecules in assays which contain disease-relevant seeds amplified from those extracts.

Through the application of a FRET-based biosensor assay, we have demonstrated that HSA is a robust, early disease biomarker in HD transgenic mice. We propose that it also might be of high value for monitoring disease onset and progression in HD patients if HSA could be quantified in biosamples whose collection is technically and ethically possible, like cerebrospinal fluid, blood or muscle tissue. Through the quantification of HSA in patient samples, the optimal time point for the initiation of clinical trials could be determined and the efficacy of therapeutic interventions could be monitored. In this way, our findings may help to develop novel disease-modifying therapeutic strategies for HD and other polyQ diseases.

ACKNOWLEDGMENTS

pBAD33-CyPet-His and pBAD33-YPet-His were gifts from Patrick S. Daugherty, University of California, Santa Barbara, USA. The expression vector for Tau pRK172 Tau40 was obtained from Michel Goedert, MRC Laboratory of Molecular Biology, Cambridge, UK. Human brain tissue for this study was provided by the Newcastle

Brain Tissue Resource (NBTR), which is funded in part by a grant from the UK Medical Research Council (G0400074) and by Brains for Dementia Research, a joint venture between the Alzheimer's Society and Alzheimer's Research UK. This work was supported by the Huntington's Disease Society of America (HDSA, HD Human Biology Project Fellowship to A. B.), the Swedish Research Council (to Å.P.) and the CHDI Foundation (to E.E.W., G.P.B, A.J.M). Additionally, this study received funding from the EC funding initiative ERA-NET NEURON, consortium "ABETA ID" funded by the German Federal Ministry for Education and Research (BMBF), grant no. 01W1301, the Berlin Institute of Health Collaborative Research Grant no. 1.1.2.a.3 "Elucidating the proteostasis network to control Alzheimer's disease" funded by the German Federal Ministry for Education and Research (BMBF), the Helmholtz Validation Fund grant no. HVF-0013 "Enabling Technologies for Drug Discovery against Protein Misfolding Diseases" funded by the Helmholtz Association, Germany, (to E.E.W.), the Stiftung Charité (to E.E.W.) and the Max Delbrück Center for Molecular Medicine in the Helmholtz Association for application-oriented research (to A. Boe. and E.E.W.). We thank Maria van Waarde-Verhagen, Zhinguang Zheng and Mary Harding for excellent technical assistance. We thank the Advanced Light Microscopy Technology Platform of Max-Delbrück-Center for Molecular Medicine, Berlin for the general and technical support. Furthermore we thank Tom Vogt and Ignacio Munoz-Sanjuan (CHDI) for their support. Icons used in **Figure 3A** were taken from Freepik.

AUTHOR CONTRIBUTIONS

A.B., A.A. and E.E.W. conceived the study and designed the experiments; A.B. and A.A. analyzed the data. A.A., R.H., I.J. and K.K. performed experiments with *in vitro*

seeds. A.A. and R.H. performed R6/2Q212, R6/2Q51 and HdhQ150 mouse tissue experiments as well as experiments with human HD samples. A.A, L.B. and F.S. performed all studies with the HD transgenic fly strains. L.D. and A.Boe. performed aggregation experiments with non-polyQ proteins. R.H. performed immunodepletion experiments and filter assays and determined the molecular weight of aggregates. A.S. performed toxicity assays with primary neurons. S.K. and B.P. labeled and analyzed EM samples. J.K. performed all experiments with nematodes. L.B. analyzed protease cleavage reactions with SDS-PAGE. B.M. performed experiments with AAV5 HTT853 injected mice. H.N. performed cell culture studies. H.K. provided cell lines. B.B. and Å.P. performed the injections of AAV vectors in FVBN/ mice and provided samples. J.M. coordinated breeding of R6/2Q51 mice and provided samples. S.F. and G.B. coordinated breeding of R6/2Q212 and *Hdh*Q150 mice and provided samples. L.B. and G.G. analyzed AFM samples. E.E.W., A.B., A.A. and S.S. conceived and wrote the manuscript.

DECLARATION OF INTERESTS

The authors declare no competing interests.

REFERENCES

Arrasate, M., Mitra, S., Schweitzer, E.S., Segal, M.R., and Finkbeiner, S. (2004). Inclusion body formation reduces levels of mutant huntingtin and the risk of neuronal death. Nature *431*, 805-810.

Atarashi, R., Moore, R.A., Sim, V.L., Hughson, A.G., Dorward, D.W., Onwubiko, H.A., Priola, S.A., and Caughey, B. (2007). Ultrasensitive detection of scrapie prion protein using seeded conversion of recombinant prion protein. Nature methods *4*, 645-650.

Atarashi, R., Satoh, K., Sano, K., Fuse, T., Yamaguchi, N., Ishibashi, D., Matsubara, T., Nakagaki, T., Yamanaka, H., Shirabe, S.*, et al.* (2011). Ultrasensitive human prion detection in cerebrospinal fluid by real-time quaking-induced conversion. Nature medicine *17*, 175-178.

Babcock, D.T., and Ganetzky, B. (2015). Transcellular spreading of huntingtin aggregates in the Drosophila brain. Proceedings of the National Academy of Sciences of the United States of America *112*, E5427-5433.

Baldo, B., Soylu, R., and Petersen, A. (2013). Maintenance of basal levels of autophagy in Huntington's disease mouse models displaying metabolic dysfunction. PloS one *8*, e83050.

Biancalana, M., and Koide, S. (2010). Molecular mechanism of Thioflavin-T binding to amyloid fibrils. Biochimica et biophysica acta *1804*, 1405-1412.

Bischof, J., Maeda, RK., Hediger, M., Karch, F., Basler, K. (2007) An optimized transgenesis system for Drosophila using germ-line-specific phiC31 integrases. Proc Natl Acad Sci 104(9):3312-7.

Brewer, GJ., Cotman, CW. (1989) Survival and growth of hippocampal neurons in defined medium at low density: advantages of a sandwich culture technique or low oxygen. Brain Res. 494(1):65-74.

Brundin, P., Melki, R., and Kopito, R. (2010). Prion-like transmission of protein aggregates in neurodegenerative diseases. Nature reviews. Molecular cell biology *11*, 301-307.

Busch, A., Engemann, S., Lurz, R., Okazawa, H., Lehrach, H., and Wanker, E.E. (2003). Mutant huntingtin promotes the fibrillogenesis of wild-type huntingtin: a potential mechanism for loss of huntingtin function in Huntington's disease. The Journal of biological chemistry *278*, 41452-41461.

Bäuerlein, FJB., Saha, I., Mishra, A., Kalemanov, M., Martínez-Sánchez, A., Klein, R., Dudanova, I., Hipp, MS., Hartl, FU., Baumeister, W., Fernández-Busnadiego, R. (2017) In Situ Architecture and Cellular Interactions of PolyQ Inclusions. Cell.171(1):179-187.

Carter, R.J., Lione, L.A., Humby, T., Mangiarini, L., Mahal, A., Bates, G.P., Dunnett, S.B., and Morton, A.J. (1999). Characterization of progressive motor deficits in mice transgenic for the human Huntington's disease mutation. The Journal of neuroscience : the official journal of the Society for Neuroscience *19*, 3248-3257.

Castilla, J., Saa, P., Morales, R., Abid, K., Maundrell, K., and Soto, C. (2006). Protein misfolding cyclic amplification for diagnosis and prion propagation studies. Methods in enzymology *412*, 3-21.

Castilla, J., Saa, P., and Soto, C. (2005). Detection of prions in blood. Nature medicine *11*, 982-985.

Chiti, F., Dobson, CM. (2017) Protein Misfolding, Amyloid Formation, and Human Disease: A Summary of Progress Over the Last Decade. Annu Rev Biochem. 86:27-68.

Ciamei, A., Detloff, P.J., and Morton, A.J. (2015). Progression of behavioural despair in R6/2 and Hdh knock-in mouse models recapitulates depression in Huntington's disease. Behavioural brain research *291*, 140-146.

Cohen, S.I., Linse, S., Luheshi, L.M., Hellstrand, E., White, D.A., Rajah, L., Otzen, D.E., Vendruscolo, M., Dobson, C.M., and Knowles, T.P. (2013). Proliferation of amyloid-beta42 aggregates occurs through a secondary nucleation mechanism. Proceedings of the National Academy of Sciences of the United States of America *110*, 9758-9763.

Cohen, S.I., Vendruscolo, M., Dobson, C.M., and Knowles, T.P. (2012). From macroscopic measurements to microscopic mechanisms of protein aggregation. Journal of molecular biology *421*, 160-171.

Colby, D.W., Zhang, Q., Wang, S., Groth, D., Legname, G., Riesner, D., and Prusiner, S.B. (2007). Prion detection by an amyloid seeding assay. Proceedings of the National Academy of Sciences of the United States of America *104*, 20914-20919.

Davies, S.W., Turmaine, M., Cozens, B.A., DiFiglia, M., Sharp, A.H., Ross, C.A., Scherzinger, E., Wanker, E.E., Mangiarini, L., and Bates, G.P. (1997). Formation of neuronal intranuclear inclusions underlies the neurological dysfunction in mice transgenic for the HD mutation. Cell *90*, 537-548.
DiFiglia, M., Sapp, E., Chase, K.O., Davies, S.W., Bates, G.P., Vonsattel, J.P., and Aronin, N. (1997). Aggregation of huntingtin in neuronal intranuclear inclusions and dystrophic neurites in brain. Science (New York, N.Y.) *277*, 1990-1993.
Du, D., Murray, A.N., Cohen, E., Kim, H.E., Simkovsky, R., Dillin, A., and Kelly, J.W. (2011). A kinetic aggregation assay allowing selective and sensitive amyloid-beta quantification in cells and tissues. Biochemistry *50*, 1607-1617.
Gao, M., Estel, K., Seeliger, J., Friedrich, R.P., Dogan, S., Wanker, E.E., Winter, R., and Ebbinghaus, S. (2015). Modulation of human IAPP fibrillation: cosolutes, crowders and chaperones. Physical chemistry chemical physics : PCCP *17*, 8338-8348.
Goedert, M. (2015). NEURODEGENERATION. Alzheimer's and Parkinson's diseases: The prion concept in relation to assembled Abeta, tau, and alpha-synuclein. Science (New York, N.Y.) *349*, 1255555.
Guo, J.L., and Lee, V.M. (2014). Cell-to-cell transmission of pathogenic proteins in neurodegenerative diseases. Nature medicine *20*, 130-138.
Gupta, S., Jie, S., and Colby, D.W. (2012). Protein misfolding detected early in pathogenesis of transgenic mouse model of Huntington disease using amyloid seeding assay. The Journal of biological chemistry *287*, 9982-9989.
Herva, M.E., Zibaee, S., Fraser, G., Barker, R.A., Goedert, M., and Spillantini, M.G. (2014). Anti-amyloid compounds inhibit alpha-synuclein aggregation induced by protein misfolding cyclic amplification (PMCA). The Journal of biological chemistry *289*, 11897-11905.
Hockly, E., Woodman, B., Mahal, A., Lewis, C.M., and Bates, G. (2003). Standardization and statistical approaches to therapeutic trials in the R6/2 mouse. Brain research bulletin *61*, 469-479.
Holmes, B.B., Furman, J.L., Mahan, T.E., Yamasaki, T.R., Mirbaha, H., Eades, W.C., Belaygorod, L., Cairns, N.J., Holtzman, D.M., and Diamond, M.I. (2014). Proteopathic tau seeding predicts tauopathy in vivo. Proceedings of the National Academy of Sciences of the United States of America *111*, E4376-4385.
Hult, S., Soylu, R., Bjorklund, T., Belgardt, B.F., Mauer, J., Bruning, J.C., Kirik, D., and Petersen, A. (2011). Mutant huntingtin causes metabolic imbalance by disruption of hypothalamic neurocircuits. Cell metabolism *13*, 428-439.
Jarrett, J.T., and Lansbury, P.T., Jr. (1993). Seeding "one-dimensional crystallization" of amyloid: a pathogenic mechanism in Alzheimer's disease and scrapie? Cell *73*, 1055-1058.
Jeon, I., Cicchetti, F., Cisbani, G., Lee, S., Li, E., Bae, J., Lee, N., Li, L., Im, W., Kim, M.*, et al.* (2016). Human-to-mouse prion-like propagation of mutant huntingtin protein. Acta neuropathologica.
Jiang, X., and Sorkin, A. (2002). Coordinated traffic of Grb2 and Ras during epidermal growth factor receptor endocytosis visualized in living cells. Molecular biology of the cell *13*, 1522-1535.
Jucker, M., and Walker, L.C. (2013). Self-propagation of pathogenic protein aggregates in neurodegenerative diseases. Nature *501*, 45-51.
Kayed, R., Head, E., Thompson, J.L., McIntire, T.M., Milton, S.C., Cotman, C.W., and Glabe, C.G. (2003). Common structure of soluble amyloid oligomers implies common mechanism of pathogenesis. Science (New York, N.Y.) *300*, 486-489.
Kim, Y.E., Hosp, F., Frottin, F., Ge, H., Mann, M., Hayer-Hartl, M., and Hartl, F.U. (2016). Soluble Oligomers of PolyQ-Expanded Huntingtin Target a Multiplicity of Key Cellular Factors. Molecular cell *63*, 951-964.
Ko, J., Ou, S., and Patterson, P.H. (2001). New anti-huntingtin monoclonal antibodies: implications for huntingtin conformation and its binding proteins. Brain research bulletin *56*, 319-329.
Kuemmerle, S., Gutekunst, C.A., Klein, A.M., Li, X.J., Li, S.H., Beal, M.F., Hersch, S.M., and Ferrante, R.J. (1999). Huntington aggregates may not predict neuronal death in Huntington's disease. Annals of neurology *46*, 842-849.
Larson, E., Fyfe, I., Morton, A.J., and Monckton, D.G. (2015). Age-, tissue- and length-dependent bidirectional somatic CAG*CTG repeat instability in an allelic series of R6/2 Huntington disease mice. Neurobiology of disease *76*, 98-111.

Latouche, M., Lasbleiz, C., Martin, E., Monnier, V., Debeir, T., Mouatt-Prigent, A., Muriel, MP., Morel, L., Ruberg, M., Brice, A., Stevanin, G., Tricoire H. (2007) A conditional pan-neuronal Drosophila model of spinocerebellar ataxia 7 with a reversible adult phenotype suitable for identifying modifier genes. J Neurosci. (10):2483-92.
Laue, M. (2010). Electron microscopy of viruses. Methods in cell biology *96*, 1-20.
Leitman, J., Ulrich Hartl, F., and Lederkremer, G.Z. (2013). Soluble forms of polyQ-expanded huntingtin rather than large aggregates cause endoplasmic reticulum stress. Nature communications *4*, 2753.
LeVine, H., 3rd (1993). Thioflavine T interaction with synthetic Alzheimer's disease beta-amyloid peptides: detection of amyloid aggregation in solution. Protein science : a publication of the Protein Society *2*, 404-410.
Li, H., Li, S.H., Cheng, A.L., Mangiarini, L., Bates, G.P., and Li, X.J. (1999). Ultrastructural localization and progressive formation of neuropil aggregates in Huntington's disease transgenic mice. Human molecular genetics *8*, 1227-1236.
Lin, C.H., Tallaksen-Greene, S., Chien, W.M., Cearley, J.A., Jackson, W.S., Crouse, A.B., Ren, S., Li, X.J., Albin, R.L., and Detloff, P.J. (2001). Neurological abnormalities in a knock-in mouse model of Huntington's disease. Human molecular genetics *10*, 137-144.
Lione, L.A., Carter, R.J., Hunt, M.J., Bates, G.P., Morton, A.J., and Dunnett, S.B. (1999). Selective discrimination learning impairments in mice expressing the human Huntington's disease mutation. The Journal of neuroscience : the official journal of the Society for Neuroscience *19*, 10428-10437.
Mangiarini, L., Sathasivam, K., Seller, M., Cozens, B., Harper, A., Hetherington, C., Lawton, M., Trottier, Y., Lehrach, H., Davies, S.W.*, et al.* (1996). Exon 1 of the HD gene with an expanded CAG repeat is sufficient to cause a progressive neurological phenotype in transgenic mice. Cell *87*, 493-506.
Meyer-Luehmann, M., Coomaraswamy, J., Bolmont, T., Kaeser, S., Schaefer, C., Kilger, E., Neuenschwander, A., Abramowski, D., Frey, P., Jaton, A.L.*, et al.* (2006). Exogenous induction of cerebral beta-amyloidogenesis is governed by agent and host. Science (New York, N.Y.) *313*, 1781-1784.
Nguyen, A.W., and Daugherty, P.S. (2005). Evolutionary optimization of fluorescent proteins for intracellular FRET. Nature biotechnology *23*, 355-360.
Nucifora, L.G., Burke, K.A., Feng, X., Arbez, N., Zhu, S., Miller, J., Yang, G., Ratovitski, T., Delannoy, M., Muchowski, P.J.*, et al.* (2012). Identification of novel potentially toxic oligomers formed in vitro from mammalian-derived expanded huntingtin exon-1 protein. The Journal of biological chemistry *287*, 16017-16028.
Osterwalder, T., Yoon, KS., White, BH., Keshishian, H. (2015) A conditional tissue-specific transgene expression system using inducible GAL4. Proc Natl Acad Sci 98(22):12596-601.
Pecho-Vrieseling, E., Rieker, C., Fuchs, S., Bleckmann, D., Esposito, M.S., Botta, P., Goldstein, C., Bernhard, M., Galimberti, I., Muller, M.*, et al.* (2014). Transneuronal propagation of mutant huntingtin contributes to non-cell autonomous pathology in neurons. Nature neuroscience *17*, 1064-1072.
Peelaerts, W., Bousset, L., Van der Perren, A., Moskalyuk, A., Pulizzi, R., Giugliano, M., Van den Haute, C., Melki, R., and Baekelandt, V. (2015). alpha-Synuclein strains cause distinct synucleinopathies after local and systemic administration. Nature *522*, 340-344.
Pieri, L., Madiona, K., Bousset, L., and Melki, R. (2012). Fibrillar alpha-synuclein and huntingtin exon 1 assemblies are toxic to the cells. Biophysical journal *102*, 2894-2905.
Rogers, I., Kerr, F., Martinez, P., Hardy, J., Lovestone, S., Partridge, L. (2012) Ageing increases vulnerability to aβ42 toxicity in Drosophila. PLoS One. 7(7):e40569.Saa, P., Castilla, J., and Soto, C. (2006). Presymptomatic detection of prions in blood. Science (New York, N.Y.) *313*, 92-94.
Saborio, G.P., Permanne, B., and Soto, C. (2001). Sensitive detection of pathological prion protein by cyclic amplification of protein misfolding. Nature *411*, 810-813.
Sahl, S.J., Weiss, L.E., Duim, W.C., Frydman, J., and Moerner, W.E. (2012). Cellular inclusion bodies of mutant huntingtin exon 1 obscure small fibrillar aggregate species. Scientific reports *2*, 895.

Salvadores, N., Shahnawaz, M., Scarpini, E., Tagliavini, F., and Soto, C. (2014). Detection of misfolded Abeta oligomers for sensitive biochemical diagnosis of Alzheimer's disease. Cell reports *7*, 261-268.
Sathasivam, K., Lane, A., Legleiter, J., Warley, A., Woodman, B., Finkbeiner, S., Paganetti, P., Muchowski, P.J., Wilson, S., and Bates, G.P. (2010). Identical oligomeric and fibrillar structures captured from the brains of R6/2 and knock-in mouse models of Huntington's disease. Human molecular genetics *19*, 65-78.
Sathasivam, K., Neueder, A., Gipson, T.A., Landles, C., Benjamin, A.C., Bondulich, M.K., Smith, D.L., Faull, R.L., Roos, R.A., Howland, D.*, et al.* (2013). Aberrant splicing of HTT generates the pathogenic exon 1 protein in Huntington disease. Proceedings of the National Academy of Sciences of the United States of America *110*, 2366-2370.
Scherzinger, E., Lurz, R., Turmaine, M., Mangiarini, L., Hollenbach, B., Hasenbank, R., Bates, G.P., Davies, S.W., Lehrach, H., and Wanker, E.E. (1997). Huntingtin-encoded polyglutamine expansions form amyloid-like protein aggregates in vitro and in vivo. Cell *90*, 549-558.
Scherzinger, E., Sittler, A., Schweiger, K., Heiser, V., Lurz, R., Hasenbank, R., Bates, G.P., Lehrach, H., and Wanker, E.E. (1999). Self-assembly of polyglutamine-containing huntingtin fragments into amyloid-like fibrils: implications for Huntington's disease pathology. Proceedings of the National Academy of Sciences of the United States of America *96*, 4604-4609.
Schindelin, J., Arganda-Carreras, I., Frise, E., Kaynig, V., Longair, M., Pietzsch, T., Preibisch, S., Rueden, C., Saalfeld, S., Schmid, B.*, et al.* (2012). Fiji: an open-source platform for biological-image analysis. Nature methods *9*, 676-682.
Silveira, JR., Raymond, GJ., Hughson, AG., Race, RE., Sim, VL., Hayes, SF., Caughey, B. (2005) The most infectious prion protein particles. Nature. 437(7056):257-61.Slow, E.J., Graham, R.K., Osmand, A.P., Devon, R.S., Lu, G., Deng, Y., Pearson, J., Vaid, K., Bissada, N., Wetzel, R.*, et al.* (2005). Absence of behavioral abnormalities and neurodegeneration in vivo despite widespread neuronal huntingtin inclusions. Proceedings of the National Academy of Sciences of the United States of America *102*, 11402-11407.
Sofola, O., Kerr, F., Rogers, I., Killick, R., Augustin, H., Gandy, C., Allen, MJ., Hardy, J., Lovestone, S., Partridge, L. (2010) Inhibition of GSK-3 ameliorates Abeta pathology in an adult-onset Drosophila model of Alzheimer's disease. PLoS Genet. 6(9):e1001087.Soto, C. (2012). Transmissible proteins: expanding the prion heresy. Cell *149*, 968-977.
Tan, Z., Dai, W., van Erp, T.G., Overman, J., Demuro, A., Digman, M.A., Hatami, A., Albay, R., Sontag, E.M., Potkin, K.T.*, et al.* (2015). Huntington's disease cerebrospinal fluid seeds aggregation of mutant huntingtin. Molecular psychiatry *20*, 1286-1293.
Taylor, J.P., Tanaka, F., Robitschek, J., Sandoval, C.M., Taye, A., Markovic-Plese, S., and Fischbeck, K.H. (2003). Aggresomes protect cells by enhancing the degradation of toxic polyglutamine-containing protein. Human molecular genetics *12*, 749-757.
Theillet, F.X., Binolfi, A., Bekei, B., Martorana, A., Rose, H.M., Stuiver, M., Verzini, S., Lorenz, D., van Rossum, M., Goldfarb, D.*, et al.* (2016). Structural disorder of monomeric alpha-synuclein persists in mammalian cells. Nature *530*, 45-50.
Wanker, E.E., Scherzinger, E., Heiser, V., Sittler, A., Eickhoff, H., and Lehrach, H. (1999). Membrane filter assay for detection of amyloid-like polyglutamine-containing protein aggregates. Methods in enzymology *309*, 375-386.
Woodman, B., Butler, R., Landles, C., Lupton, M.K., Tse, J., Hockly, E., Moffitt, H., Sathasivam, K., and Bates, G.P. (2007). The Hdh(Q150/Q150) knock-in mouse model of HD and the R6/2 exon 1 model develop comparable and widespread molecular phenotypes. Brain research bulletin *72*, 83-97.
Zhang, J.H., Chung, T.D., and Oldenburg, K.R. (1999). A Simple Statistical Parameter for Use in Evaluation and Validation of High Throughput Screening Assays. Journal of biomolecular screening *4*, 67-73.
Zuccato, C., Valenza, M., and Cattaneo, E. (2010). Molecular mechanisms and potential therapeutical targets in Huntington's disease. Physiological reviews *90*, 905-981.

FIGURES LEGENDS

Figure 1. Establishment of a FRET-based HTT aggregate seeding assay

(A) Analysis of the aggregation propensity of proteolytically cleaved GST-Ex1Q48-CyPet and -YPet fusion proteins. Both sensor proteins (3 µM) were individually incubated at 25 °C with PreScission protease (PSP); time-dependent formation of SDS-resistant aggregates was analyzed by FRA. A polyclonal anti-GFP antibody recognizing both tags (CyPet and YPet) was used for visualization of spontaneously formed aggregates.

(B) Atomic force microscopy (AFM) analysis of spontaneously formed Ex1Q48-CyPet, Ex1Q48-YPet and Ex1Q48 aggregates (3 µM) after 24 h. Scale bars: 1 µm; color gradient represents 0-20 nm height.

(C) Schematic model of the spontaneous FRET-inducing Ex1Q48-CyPet/-YPet co-aggregation reaction in cell-free assays. Initially, the N-terminal GST-tag keeps the fusion proteins in a soluble state and prevents spontaneous aggregation. After PSP-mediated cleavage of the fusion proteins, Ex1Q48-CyPet and -YPet fragments are released and spontaneously co-aggregate over time. Co-aggregation is monitored by quantification of FRET, arising when fluorescent tags come into close proximity in ordered protein aggregates.

(D) Investigation of spontaneous co-aggregation of sensor proteins by time-dependent quantification of FRET. Various concentrations of the sensor proteins Ex1Q48-CyPet and -YPet (1:1 mixture) were incubated at 25 °C in the presence and absence of PSP. The initial FRET signal of ~6% is due to oligomerization of uncleaved fusion proteins under non-denaturating conditions. FRET efficiency is displayed as mean ± SD of technical triplicates.

(E) Preformed, fibrillar Ex1Q48 aggregates (seeds) induce a concentration-dependent acceleration of Ex1Q48-CyPet/-YPet (1.2 µM) polymerization in cell-free

assays. Co-aggregation of the fluorescence sensor proteins was monitored by quantification of FRET for 30 h; the resulting aggregation kinetics were curve fitted by non-linear regression. Indicated seed concentrations are equivalent to initially applied monomer concentrations. FRET efficiency is displayed as mean ± SD of technical triplicates.

(F) Calculation of Δt_{50} values from aggregation profiles of seeded and unseeded reactions in **E**. HTT seeding activity (HSA) is detected in a concentration-dependent manner when preformed fibrillar Ex1Q48 aggregates are added to reactions. Δt_{50} is displayed as individual values (black ●) and mean ± SD of technical triplicates.

Figure 2. FRASE assays facilitate the detection of preformed Ex1Q48 seeds with high specificity and sensitivity

(A) Analysis of sonicated (1 min) and non-sonicated preformed fibrillar Ex1Q48 aggregates by blue native (BN) PAGE and immunoblotting using the HD1 antibody.

(B) Defining the detection limit of FRASE assays. A dilution series of sonicated Ex1Q48 seeds was systematically analyzed; seed concentrations were calculated using an average aggregate size of 1250 kDa. Ex1Q48-CyPet/-YPet (1.2 µM). Data are mean ± SEM (n = 5).

(C) Calculation of Δt_{50} values from aggregation profiles in **B** results in a detection threshold for sonicated Ex1Q48 seeds of ~60 fM. The assay responds quantitatively to added seeds over more than four orders of magnitude (r^2 = 0.988). Above a seed concentration of 556 fM the Z' factor exceeds 0.5. Data are mean ± SEM (n = 5).

(D) The FRASE assay specifically responds to preformed Ex1Q48 aggregates. Fibrillar aggregates prepared of amyloidogenic non-polyQ polypetides do not accelerate the co-aggregation of the reporter proteins Ex1Q48-CyPet/-YPet. Data are mean ± SD of triplicates.

(E) Analysis of preformed amyloidogenic α-synuclein (α-Syn), amyloid-β42 (Aβ), islet amyloid polypeptide (IAPP) and Tau (Tau40) protein aggregates by AFM. Scale bars: 1 µm; color gradients represent the following heights: 0-10 nm (α-Syn), 0-5 nm (Aβ), 0-30 nm (IAPP) and 0-10 nm (Tau40).

Figure 3. Detection of mutant HTT seeding activity in brain extracts of HD patients and presymptomatic HD mice

(A) Schematic representation of the FRASE assay workflow for detecting HSA in tissue homogenates. Tissues of interest are homogenized in detergent-free lysis buffer and cleared from cell debris by low-speed centrifugation. Fluorescent protein-tagged Ex1Q48 sensor proteins are supplemented with defined amounts of prepared crude protein extracts. Subsequently, co-aggregation of the sensor proteins is monitored in 384-well plates by quantification of FRET. The presence of mutant HTT seeds in the analyzed biosamples shortens the lag phase of spontaneous Ex1Q48-CyPet/-YPet co-aggregation. HSA (Δt_{50}) in tissue samples is calculated from Ex1Q48-CyPet/-YPet aggregation profiles of seeded and non-seeded reactions.

(B) FRASE analysis of brain homogenates prepared from an R6/2Q212 transgenic mouse and wild-type littermate control. The concentration of the sensor proteins GST-Ex1Q48-CyPet/-YPet was 3 µM. Data is presented as mean ± SD of technical triplicates.

(C) Calculation of Δt_{50} values from aggregation profiles in **B**. Statistical significance was assessed by two-way ANOVA followed by Bonferroni's multiple comparison post hoc test against the respective WT controls. Δt_{50} is displayed as individual values (black ●) and as mean ± SD of technical triplicates. Comparable results were obtained in two independent experiments.

(D) Quantification of HSA in brain homogenates prepared from cerebellum, caudate nucleus and cerebral cortex of HD patients and controls with FRASE assays. For clarity, the average Δt_{50} values obtained from six healthy control samples are depicted. Individual values of Δt_{50} (black ●) and mean ± SD of triplicates are displayed.

(E) Quantification of mutant HSA in brain extracts prepared from R6/2Q212 transgenic mice. Mice were sacrificed at the indicated age (3 mice per age); brain extracts were analyzed using the FRASE assay. Corresponding extracts from wild-type (WT) littermate controls were analyzed for all ages; an average Δt_{50} value was depicted for clarity.

(F) Analysis of sonicated brain extracts prepared from young R6/2Q212 transgenic mice using the FRASE assay. Results from corresponding littermates are shown as an average Δt_{50} value.

(G) Investigation of brain extracts prepared from indicated brain regions of *Hdh*Q150 heterozygous knock-in mice. Corresponding extracts from 2-, 5- and 8-month-old WT mice were also analyzed and average Δt_{50} values are depicted for clarity. Data are mean ± SEM (n = 3). The concentration of the sensor proteins GST-Ex1Q48-CyPet/-YPet in (D), (E), (F) and (G) is 1.2 µM. In (E), (F) and (G) HSA measured for each mouse is displayed as black ●. Bars are mean ± SEM. Statistical significance was assessed by One-Way ANOVA followed by Dunnett's multiple comparisons test.

Figure 4. Small fibrillary HTT aggregates prepared from R6/2Q212 mouse brain are highly seeding competent

(A) Scheme of the different centrifugation steps applied to prepare soluble and insoluble fractions from brain homogenates of R6/2Q212 transgenic mice.

(B) Quantification of HSA in soluble and insoluble fractions prepared by centrifugation from crude brain homogenates using FRASE assays. In all cases, data obtained for transgenic mice were normalized to age-matched wild-type control mice. Bars are mean ± SEM (n = 2). HSA measured for each mouse is displayed as black ●.

(C) Analysis of soluble and insoluble fractions prepared by centrifugation from mouse brain homogenates using a denaturing FRA.

(D) Analysis of the P2 fraction after high-speed centrifugation by immunoelectron microscopy. The P2 fraction was prepared from 9-week-old R6/2Q212 transgenic mice and age-matched wild-type (WT) controls. Fibrillar HTT aggregates were visualized with the anti-Agg53 HTT antibody and a gold-labeled secondary antibody. Scale bar corresponds to 100 nm.

Figure 5. The short-term mHTT-expression-induced decrease in *Drosophila* lifespan correlates with HSA but not with aggregate load in general

(A) Scheme of temporary hormone treatment. The black lines indicate time periods of hormone treatment (RU486 food); the grey lines indicate time periods without hormone treatment (normal food). Treatment started at day three post-eclosion.

(B) Life span analysis of GS;HTTex1Q97 and GS;HTTex1Q17 flies expressing the respective transgene for 0d (OFF; $n^{GS;HTTex1Q97}$ = 99, 96, 107; $n^{GS;HTTex1Q17}$ = 107, 102, 100), 3d (3d-ON/OFF; $n^{GS;HTTex1Q97}$ = 107, 108, 107; $n^{GS;HTTex1Q17}$ = 109, 96, 97), 6d (6d-ON/OFF; $n^{GS;HTTex1Q97}$ = 108, 105, 94; $n^{GS;HTTex1Q17}$ = 110, 97, 100) or permanently (ON; $n^{GS;HTTex1Q97}$ = 102, 98, 106; $n^{GS;HTTex1Q17}$ = 100, 109, 101). Life span is plotted as the percentage of surviving flies of three biological replicates.

(C) Median life span calculated from survival curves in **B**. Average survival of each experiment (n = ~ 100 flies) is presented as black ●. Bars are mean ± SEM from three independent replicates; Statistical significance was assessed by One-way

ANOVA Dunnett's post-hoc test; data were compared to GS;HTTex1Q97^{OFF} transgenic flies [statistically significant differences are indicated by asterisks (*)] or to GS;HTTex1Q97^{ON} flies [statistically significant differences are indicated by hashtags (#)]; ns, not statistically significant; */# $p < 0.05$; **/## $p < 0.01$; ***/### $p < 0.001$.

(D) Analysis of motor performance of GS;HTTex1Q97 flies expressing the respective transgene for 0d (OFF), 3d (3d-ON/OFF), 6d (6d-ON/OFF) or permanently (ON). Results are presented as mean of three independent replicates each starting with 100 flies per condition.

(E) Quantification of HTT aggregate load in fly heads by FRAs immunodetected with the MW8 antibody. Representative images for each condition are shown below the bar graph. Data are displayed as mean ± SEM; Individual measurements are presented as black ●; One-way ANOVA Dunnett's post hoc test.

(F) FRASE analysis of head lysates from flies analyzed in **E**. Values are plotted as means ± SEM of three biological replicates each performed in triplicates.

(G) HSA calculated from aggregation kinetics in **F**. Results are displayed as mean ± SEM; Individual measurements are presented as black ●; One-way ANOVA Dunnett's post hoc test compared to GS;HTTex1Q97^{OFF} flies.

(H) Pearson correlation analysis shows a significant linear relationship between *Drosophila* lifespan and HSA assessed by FRASE assays ($p = 0.020$), whereas *Drosophila* lifespan does not correlate with the aggregate load detected by FRAs [$p = 0.368$ (FRA,MAB5492), $p = 0.411$ (FRA, MW8)]. All data are presented as mean ± SEM of the three individual experiments.

Figure 6. Co-expression of the human molecular chaperone Hsp70 reduces HSA and HTTex1Q97 induced toxicity in HD transgenic flies

(A) Scheme of temporary hormone treatment. The orange/green lines indicate time periods of hormone treatment (RU486 food); the grey lines indicate time periods without hormone treatment (normal food). Treatment started at day three post-eclosion.

(B) Life span analysis of GS;HTTex1Q97 and GS;HSPA1L;HTTex1Q97 flies expressing the respective transgenes for 6d (6d-ON/OFF; $n^{GS;HTTex1Q97}$ = 108, 105, 94; $n^{GS;HSPA1L;HTTex1Q97}$ = 103, 82, 83). As comparison the survival curve of untreated GS;HTTex1Q97 (OFF) from **5B** is shown. Life span is plotted as the percentage of surviving flies of three biological.

(C) Median life span calculated from survival curves in **B**. Average survival of individual experiments (n = ~ 100 flies) is presented as black ●. Bars are mean ± SEM from three independent replicates; Statistical significance was assessed by unpaired t test.

(D) Quantification of HTT aggregate load in fly heads by FRAs immunodetected with the MW8 antibody. Representative images for each condition are shown below the bar graph. Data are displayed as mean ± SEM; Individual measurements are presented as black ●; Statistical significance was assessed by unpaired t test.

(E) FRASE analysis of fly head lysates. Values are plotted as mean ± SEM of three biological replicates each performed in triplicates.

(F) HSA calculated from aggregation kinetics in **E**. Results are displayed as mean ± SEM; Individual measurements are presented as black ●; Statistical significance was assessed by unpaired t test.

(G) Representative confocal images of the right central brain regions GS;HSPA1L;HTTex1Q97 treated for 6 days with RU486 immunostained for HTT (Mab5492, green) and Hsp70 (anti-HSP70/HSP72, red). White arrows indicate co-localization of HSPA1L with HTT aggregates. Grey arrow indicates areas in the

brain where Hsp70 is not associated with HTT aggregates. Scale bars: 20 µm.

Figure S1 related to Figure 1: Characterization of HTTex1 sensor proteins

(A) Schematic representation of the applied GST-tagged HTTex1 fusion proteins with pathogenic and non-pathogenic polyQ tracts. P, proline-rich regions.

(B) The recombinant GST-Ex1Q48-CyPet and -YPet fusion proteins were affinity purified using glutathione-coated sepharose beads. Purity was assessed by SDS-PAGE and subsequent Coomassie blue staining.

(C) Investigation of the PreScission protease (PSP)-mediated cleavage of the GST tag from the GST-Ex1Q48-CyPet and -YPet fusion proteins. 3 µM of GST fusion proteins were incubated in the presence or absence of the protease. Aliquots were taken at the indicated time points; cleavage was confirmed by SDS-PAGE and immunoblotting with a polyclonal anti-GFP antibody.

(D) AFM analysis of the co-aggregated sensor proteins Ex1Q48-CyPet/-YPet (3 µM). Scale bars: 1 µm; color gradient represents 0-20 nm height.

(E) Preformed, fibrillar Ex1Q48 aggregates (seeds) induce acceleration of Ex1Q48-CyPet/-YPet polymerization but do not induce aggregation of Ex1Q23-CyPet/-YPet. Seeds were produced by incubating GST-Ex1Q48 fusion protein with PSP for 24 h at 25°C. Indicated seed concentrations are equivalent to initially applied monomer concentrations. Co-aggregation of the fluorescence sensor proteins (1.2 µM) was monitored by quantification of FRET for 30 h; the resulting aggregation kinetics were curve fitted by non-linear regression. FRET efficiency is plotted as means ± SD of three technical replicates.

(F) Ex1Q48-CyPet/-YPet (3µM) sensor protein co-aggregation was accelerated by the addition of preformed fibrillary Ex1Q48 seeds. Ex1Q23 was prepared under identical condition (no fibrillar aggregates observed; data not shown) but did not

accelerate the co-aggregation of Ex1Q48-CyPet/-YPet sensor proteins. Likewise, the co-aggregation of sensor proteins was not influenced by the addition of uncleaved GST-Ex1Q48 or GST-Ex1Q23, respectively. Co-aggregation of the fluorescence sensor proteins was monitored by quantification of FRET for 12 h; the resulting aggregation kinetics were curve fitted by non-linear regression. Indicated seed concentrations are equivalent to initially applied monomer concentrations. Data is shown as means ± SD of three technical replicates.

Figure S2 related to Figure 2. Both small and large fibrillar Ex1Q48 aggregates exhibit HTT seeding activity in FRASE assays

(A) Sonication of preformed, fibrillar Ex1Q48 aggregates reveals protein fractions with high HSA in FRASE assays. Fibrillar Ex1Q48 aggregates were produced by incubating GST-Ex1Q48 fusion protein (2 μM) for 24 h at 25°C. 1 nM preformed Ex1Q48 aggregates were added to reactions (Ex1Q48-CyPet/-YPet sensor protein concentration = 1.2 μM). The added seed concentration is equivalent to the initially applied monomer concentration. Data is shown as means ± SD of three technical replicates.

(B) Calculated Δt_{50} values from Ex1Q48-CyPet/-YPet aggregation profiles in **A**. Δt_{50} is displayed as individual values (black ●) and mean ± SD of technical triplicates.

(C) Analysis of sonicated and non-sonicated Ex1Q48 seeds by denaturing filter retardation (FRA, left panel) and dot blot (DB, right panel) assays. Fragmentation of large fibrillar Ex1Q48 aggregates by sonication prevents their detection in FRAs.

(D) Preformed Ex1Q48 fibrils were sonicated for the indicated times and visualized by AFM. Sonication reduces the size of preformed fibrillar Ex1Q48 aggregates. Scale bar: 1 µm; color gradient represents 0-20 nm height.

Figure S3 related to Figure 3. Detection of mutant HTT seeding activity in brain extracts of various HD mouse models

(A) Mouse brain homogenates (7.5 μg) prepared from R6/2Q212 and WT were added to Ex1Q48-CyPet/-YPet or Ex1Q23-CyPet/-YPet sensor proteins. R6/2Q212 brain homogenates accelerate Ex1Q48-CyPet/-YPet polymerization but do not induce co-aggregation of Ex1Q23-CyPet/-YPet proteins. Co-aggregation of the fluorescence sensor proteins (1.2μM) was monitored by quantification of FRET for 30 h and displayed as mean ± SD of technical triplicates; the resulting aggregation kinetics were curve fitted by non-linear regression.

(B) Analysis of brain extracts prepared from R6/2Q51 transgenic mice and controls using FRASE assays (1.2 μM Ex1Q48-CyPet/-YPet). HSA measured for each mouse is displayed as black ●. Bars are mean ± SEM. Statistical significance was assessed by One-Way ANOVA followed by Dunnett's multiple comparisons test (n = 2).

(C) Analysis of body weight of FVB/N mice expressing the proteins HTT853Q18 or HTT853Q79 for 8 weeks. Body weight of individual mice is displayed as black ●. Bars are mean ± SEM. Statistical significance was assessed by One-Way ANOVA followed by Dunnett's multiple comparisons test (n = 3).

(D) Quantification of HSA in hypothalamic brain homogenates of FVB/N mice expressing the proteins HTT853Q18 or HTT853Q79. The concentration of sensor proteins was 3 μM. Data are mean ± SEM (n = 3). Individual measurements are displayed as black ●. Statistical significance was assessed by One-Way ANOVA followed by Dunnett's multiple comparisons test.

(E) Brain homogenates prepared from caudate nucleus of HD patients and from temporal cortex of AD patients were analyzed by FRASE assays and compared to

corresponding brain tissue of control individual. HSA values are plotted individually (black ●) and as mean ± SEM (n = 3); caudate tissue from HD patients (Grade 4, CAG repeat length: 52.3 ± 1.2, Age 42.3 ± 2.1), caudate tissue from controls (Age 60.3 ± 1.2), cortical tissue from AD patients (Braak 6, Age 73.3 ± 4.6), cortical tissue from controls (Braak 0, Age 66.3 ± 7). Statistical significance was assessed by unpaired t test.

Figure S4 related to Figure 3. Immunodepletion of HTT aggregates from mouse brain homogenates decreases HSA in FRASE assays

(A) Immunodepletion of mutant HTT aggregates from R6/2Q212 mouse brain homogenates decreases their seeding activity in FRASE assays. Brain homogenates prepared from transgenic mice and littermate controls (12 weeks) were incubated with MW8 antibody-coated protein G beads; supernatant (post-IP) and input samples were applied to FRASE analysis using 3 μM of sensor proteins. FRET efficiency is plotted as mean ± SD of technical triplicates.

(B) Same procedure as in **A** but with an IgG isotype control antibody.

(C and D) Immunoblots of samples analyzed in A and B. HTT aggregates appear as a smear at the upper edge of the blot (red rectangles). Input, brain extract before immunodepletion; Sup, supernatant after immunodepletion; Beads, antibody-coated protein G beads after immunodepletion. HTT aggregates are depleted from mouse brain homogenates with the anti-HTT antibody MW8 but not with an IgG isotype control antibody.

Figure S5 related to Figure 5. Temporal regulation of HTTex1Q97 transgene expression in newly generated *Drosophila* models of HD

(A) Confirmation of strain identity of HTTex1Q17 and HTTex1Q97 flies by PCR-based genotyping. Expected sizes of PCR products: 526 bp (HTTex1Q17) and 766 bp (HTTex1Q97).

(B) Life span analysis of w1118;HTTex1Q97 and w1118;HTTex1Q17 flies ($n^{w1118;HTTex1Q17}$ = 92, 176, 98; $n^{w1118;HTTex1Q17}$ = 88, 148, 93). Life span is plotted as the percentage of surviving flies of three biological replicates.

(C) Schematic illustration of The GAL4 / UAS and the Gene-Switch expression system. The yeast transcription activator GAL4 binds to the UAS sequence and activates the transcription of the transgene (TG) cloned downstream of the UAS. The Gene-Switch system is based on a of GAL4-progesterone receptor fusion protein which is not transcriptionally active until induced by steroids (RU486). This allows temporary regulation of transgene expression.

(D) Schematic illustration of the RU486 treatment used to induce HTTex1Q97 expression. Grey lines, no treatment; black lines, RU486 treatment.

(E) qPCR analysis of induction of HTTex1Q97 transcription upon treatment with the inducer hormone RU486. The rp49 gene was used as reference gene. Results are depicted individually (black ●) and as mean ± SEM of three biological replicates; Statistical significance was assessed by One-way ANOVA Dunnett's post-hoc test.

(F) Analysis of HTT aggregate load in fly heads by FRAs immunodetected with the MW8 antibody. Two biological replicates are depicted per condition.

(G) FRASE analysis of head lysates from flies analyzed in **F**. Values are plotted as means ± SEM of three biological replicates each performed in triplicates.

Figure S6 related to Figure 5. Detection of HTT aggregates in *Drosophila* HD models

(A) Illustration of hormone treatment utilized to assess the dynamics of HTTex1Q97 transcriptional repression upon hormone removal. Grey lines indicate time periods without RU486 treatment and black lines indicate time periods of exposure to RU486.

(B) Relative mRNA levels assessed by qPCR show transcriptional repression of HTTex1Q97 upon removal of RU486. Values are depicted as mean ± SEM of three biological replicates; individual measurements (black ●); significance assessment with One-way ANOVA Dunnett's post-hoc test.

(C) Treatment scheme for the preparation of Drosophila samples for FRA and FRASE analyses.

(D) Analysis of HTT aggregate load in fly head lysates by FRAs (75 µg protein) using the MAB5492 antibody. Data is displayed as mean ± SEM of three biological replicates; individual measurements (black ●); Statistical significance was assessed by One-way ANOVA Dunnett's post-hoc test.

(E) Representative confocal images of elavGS;HTTex1Q97 whole fly brains (hormone treatment as in **C**). The RBP staining is shown in magenta and the MAB5492 staining in green (Scale bars: 200 µm). Magnifications are shown below (Scale bars: 20 µm).

Figure S7 related to Figure 6. Analysis of HTTex1Q97 and Hsp70 expression in elavGS;HTTex1Q97 and elavGS;HSPA1L;HTTex1Q97 flies

(A) Relative mRNA levels assessed by qPCR show similar expression of HTTex1Q97 in elavGS;HTTex1Q97 and elavGS;HSPA1L;HTTex1Q97. Bars are mean ± SEM of three biological replicates and individual measurements are displayed as black ●; significance assessment with unpaired t test.

(B) Comparison of HSPA1L protein levels in elavGS;HSPA1L;HTTex1Q97 and elavGS;HSPA1L flies untreated and treatment with ru-486. Protein extracts prepared from fly heads were analyzed in SDS-PAGE and immunoblotting (20 µg of total protein).

Figure S8 related to Figure 6. Increased Q35-YFP seeding activity is associated with impairment of motility in transgenic worms

(A) Motility phenotype (% motility) of RNAi-treated and untreated Q35-YFP expressing transgenic worms at day 5 of adulthood. In all cases, data were normalized to age-matched control worms. Data are mean ± SEM (n=20). Significance assessment with unpaired t test.

(D) FRASE analysis of Q35-YFP seeding activity in RNAi-treated and untreated worms at day 5 of adulthood. FRET efficiency is displayed as mean ± SD.

(E) Quantification of results shown in **D**. HSA values are plotted individually (black ●) and as mean ± SD.

STAR * METHODS

KEY RESOURCES TABLE

REAGENT or RESOURCE	SOURCE	IDENTIFIER
Antibodies		
Rabbit polyclonal anti-GFP	Abcam	Cat#: ab290
Rabbit polyclonal anti-HTT (HD1)	Own production	Scherzinger et al., 1999
Mouse monoclonal anti-HTT (clone MW8)	DSHB	Cat#: MW8
Rabbit polyclonal anti-Agg53	This paper	N/A
Goat polyclonal anti-HTT (N18)	Santa Cruz	Cat#: sc-8767
Mouse monoclonal anti-HTT (clone 2B4)	Merck Millipore	Cat#: Mab5492
Rabbit polyclonal anti-HSP70/HSP72	Enzo Life Science	Cat#: ADI-SPA-812-D
Bacterial and Virus Strains		
BL21-CodonPlus(DE3)-RP	Integrated Science	Cat#: 230255
Biological Samples		
Post mortem brain tissues from human HD and AD patients and unaffected control individuals	Newcastle Brain Tissue Resource	
Chemicals, Peptides, and Recombinant Proteins		
GST-HTTex1Q23	This paper	N/A
GST-HTTex1Q48	Wagner et al., 2018	N/A
GST-HTTex1Q23-CyPet	This paper	N/A
GST-HTTex1Q23-YPet	This paper	N/A
GST-HTTex1Q48-CyPet	Wagner et al., 2018	N/A
GST-HTTex1Q48-YPet	Wagner et al., 2018	N/A
αSyn	Theillet et al., 2016	N/A
Tau40	InVivo BioTech Services	N/A
Mifepristone ru-486	Sigma	Cat#: M8046-1G
M-MLV Reverse Transcriptase	Thermo Scientific	Cat#: 28025013
Critical Commercial Assays		
Pierce™ BCA Protein Assay Kit	Thermo Scientific	Cat#: 23225
DNeasy® Blood & Tissue Kit	Qiagen	Cat#: 69504
TRIzol™ Reagent	Invitrogen	Cat#: 15596026
SYBR Green PCR Master Mix	Thermo Scientific	Cat#: 4309155
Deposited Data		
Experimental Models: Cell Lines		
Experimental Models: Organisms/Strains		
Mouse: R6/2Q210	Mangiarini et al., 1996	N/A
Mouse: CBA x C57Bl/6	Harlan Olac, Bicester, UK	B6CBAF1/OlaHsd
Mouse: HdhQ150	Lin et al., 2001	N/A
Mouse: R6/2Q51	Larson et al., 2015	N/A
Mouse: FVB/N		
Fly: Elav^{c115}-GAL4	Lin et al., 1994	N/A

Fly: GSelav-GAL4	Bloomington Drosophila Stock Center	Bloomington Stock 43642
Fly: HTTex1Q17	This paper	N/A
Fly: HTTex1Q97	This paper	N/A
Fly: HSPA1L	Warrick et al., 1999	N/A
Oligonucleotides		
HTTex1Q48 no Stop forward primer: 5'-gacgacgaattcatggcgaccctg-3'	This paper	N/A
HTTex1Q48 no Stop reverse primer: 5'- gacgacctcgagtggtcggtgcagcgg-3'	This paper	N/A
CyPet forward primer: 5'-acgacctcgagggtggcggtggcggtatgtctaaag gtgaagaattattcgg-3'	This paper	N/A
CyPet reverse primer: 5'- gacgacgcggccgcttatttgtacaattcatccatacc atg-3'	This paper	N/A
YPet forward primer: 5'-gacgacctcgagggtggcggtggcggtatgtctaaa ggtgaagaattattcactgg-3'	This paper	N/A
YPet reverse primer: 5'- gacgacgcggccgcttatttgtacaattcattcataccc tcg-3'	This paper	N/A
HTTex1Q23 no Stop forward primer: 5'-gacgacgaattcatggcgaccctg-3'	This paper	N/A
HTTex1Q23 no Stop reverse primer: 5'-gacgacgcggccgcctcgagtggtcggtg cagcgg-3'	This paper	N/A
HTTex1Q23 forward primer: 5'-gacgacgaattcatggcgaccctg -3'	This paper	N/A
HTTex1Q23 reverse primer: 5'-gacgacgcggccgcctcgagttatggtcggtgcagcgg-3'	This paper	N/A
Drosophila genotyping forward primer: 5'-aaccccgtaaatcaactgc- 3'	This paper	N/A
Drosophila genotyping reverse primer: 5'-atctctgtaggtagtttgtc-3'	This paper	N/A
HTTqPCR forward primer: 5′-gacctggaaaagctgatga-3′	This paper	N/A
HTTqPCR reverse primer: 5′-tcatggtcggtgcagcggct-3′	This paper	N/A
rp49qPCR forward primer: 5′-tacaggcccaagatcgtgaa-3′	This paper	N/A
rp49qPCR reverse primer: 5′-acgttgtgcaccaggaactt-3′	This paper	N/A
Recombinant DNA		
pBAD33-CyPet-His	Addgene	Addgene plasmid #14030
pBAD33-YPet-His	Addgene	Addgene plasmid #14031
Software and Algorithms		
AIDA Image Analyzer v.3.21A	AIDA	N/A
GraphPad Prism	GraphPad software	N/A
JPK SPM software	JPK Instruments	N/A
Other		

CONTACT FOR REAGENT AND RESOURCE SHARING

Further information and requests for reagents may be directed to, and will be fulfilled by the corresponding author Erich E. Wanker (ewanker@mdc-berlin.de).

EXPERIMENTAL MODEL AND SUBJECT DETAILS

HD mouse models

Hemizygous R6/2Q212 mice (Mangiarini et al., 1996) were bred by backcrossing R6/2Q212 males to (CBA x C57Bl/6) F1 females (B6CBAF1/OlaHsd, Harlan Olac, Bicester, UK). *Hdh*Q150 heterozygous knock-in mice (Lin et al., 2001; Woodman et al., 2007) on a (CBA x C57Bl/6) F1 background were generated by intercrossing *Hdh*Q150 heterozygous CBA/Ca and C57BL/6J congenic lines (inbred lines from Harlan Olac, Bicester, UK). All animals were subject to a 12 h light/dark cycle with unlimited access to drinking water and breeding chow (Special Diet Services, Witham, UK). Housing conditions and environmental enrichment were described previously (Hockly et al., 2003). R6/2 mice were always housed with wild-type mice. The CAG repeat size of the R6/2Q212 mice used in this study was 212 ± 5.27 (s.d.) and that of the *Hdh*Q150 heterozygotes was 160 ± 2.86 (s.d.). Hemizygous R6/2Q51 mice were derived from R6/2 parent lines by selective breeding (Larson et al., 2015) and bred by backcrossing R6/2Q51 males to (CBA x C57Bl/6) F1 females (Charles Rivers, UK). R6/2Q51 mice were maintained and bred as described previously (Larson et al., 2015). Female mice from the FVB/N strain were injected at eight to ten weeks of age with recombinant adeno-associated viral (AAV) vectors of serotype 5 encoding the first 853 amino acids of either the WT form of HTT with 18Q (HTT853-18Q) or the mutant form of the protein with 79Q (HTT853-79Q) (Baldo et al., 2013). All mice were housed in groups at a 12 h light/dark cycle. At eight weeks post-

injection, FVB/N mice were sacrificed. Overall, mice were sacrificed at different ages from 1 day up to two years. Tissues were strictly stored at -80 °C until use.

All animal work with R6/2Q212 and *Hdh*Q150mice was approved by the King's College London Ethical Review panel and performed under a Home Office project license in accordance with the United Kingdom 1986 Animals (Scientific procedures) Act. All animal work with R6/2Q51 mice was approved by the University of Cambridge Ethical Review panel and performed under a Home Office project license in accordance with the United Kingdom 1986 Animals (Scientific procedures) Act. All experimental procedures with FVB/N mice were approved by the Regional Ethical Committee in Lund, Sweden.

Human brain tissue

Post mortem brain tissues from human HD and AD patients and unaffected control individuals (both male and female) were obtained from the Newcastle Brain Tissue Resource (NBTR, Newcastle University, UK). Experiments were performed in accordance with the approval of the joint Ethics Committee of Newcastle and North Tyneside Health Authority and following NBTR brain banking procedures. Tissues were collected at 34.5 ± 21.0 h post-mortem from HD patients and controls with an average age of 57.8 ± 10.7 years.

Generation and maintenance of *Drosophila* strains

ElavGS-GAL4, Elav-GAL4 and HSPA1L lines were obtained from the Bloomington Drosophila Stock Center. Transgenic flies were generated through cloning of cDNAs encoding HTTex1Q17 and HTTex1Q97 into pUAST-attB-rfA (provided by Prof.

Sigrist, Freie Universität, Berlin) and subsequent site-directed insertion on the third chromosome (68E) using the PhiC31 integrase [Rainbow Transgenic Flies Inc. (Camarillo, CA, USA)]. All *Drosophila* strains were cultured on standard medium at 25°C and 65% humidity with a twelve-hour light-dark cycle. Expression of transgenes was induced by culturing flies on standard medium containing 400 µM RU486.

C. elegans strains and maintenance

C. elegans Q35 AM140 (rmIs132 (*unc*-54p::Q35::YFP)) were grown on NGM plates seeded with the *E. coli* OP50 strain at 20 °C. Nematodes were transferred to fresh wells or plates every day in the course of the experiment to separate them from their progeny.

METHOD DETAILS

Cloning of expression vectors

For the construction of plasmids encoding CyPet- and YPet-tagged HTTEx1Q48 fusion proteins, the coding sequence of HTTEx1Q48 was PCR-amplified from pGEX-6P1-HTTEx1Q48 using the primers 5'-gacgacgaattcatggcgaccctg-3' and 5'-gacgacctcgagtggtcggtgcagcgg-3'. The resulting PCR product was digested with the restriction enzymes EcoRI and NotI. Additionally, CyPet cDNA was PCR amplified from pBAD33-CyPet-His (Addgene plasmid #14030) (Nguyen and Daugherty, 2005) with the primers 5'-acgacctcgagggtggcggtggcggtatgtctaaaggtgaagaattattcgg-3' and 5'- gacgacgcggccgcttatttgtacaattcatccataccatg-3'. YPet cDNA was amplified from pBAD33-YPet-His (Addgene plasmid #14031) (Nguyen and Daugherty, 2005) with the primers 5'-gacgacctcgagggtggcggtggcggtatgtctaaaggtgaagaattattcactgg-3' and

5'- gacgacgcggccgcttatttgtacaattcattcataccctcg-3'. The resulting PCR fragments were cloned into the plasmids pGEX-6P1 using the EcoRI/XhoI/NotI restriction sites to obtain plasmids pGEX-6P1-HTTEx1Q48-CyPet and -YPet, respectively. To generate the plasmids encoding GST-Ex1Q23-CyPet and -YPet or GST-Ex1Q23 the coding sequence of HTTEx1Q23 was PCR-amplified from pDONR221-HTTEx1Q23 using the primers 5'-gacgacgaattcatggcgaccctg-3' and 5'-gacgacgcggccgcctcgagtggtcggtg cagcgg-3' (GST-Ex1Q23-CyPet and -YPet) or 5'-gacgacgaattcatggcgaccctg -3' and 5'-gacgacgcggccgcctcgagttatggtcggtgcagcgg-3'. The resulting PCR products were digested using EcoRI and XhoI endonucleases and cloned into the plasmids pGEX-6P1-HTTEx1Q48-CyPet, -YPet or pGEX-6P1-HTTEx1Q48 after excision of HTTEx1Q48 fragments by EcoRI/XhoI endonucleases.

Recombinant protein expression

The proteins GST-Ex1Q23, -Ex1Q48, -Ex1Q23-CyPet, -Ex1Q23-YPet, -Ex1Q48-CyPet and -Ex1Q48-YPet were produced in *E. coli* BL21-CodonPlus-RP and affinity-purified on glutathione-sepharose beads. Purified proteins were dialyzed over night at 4 °C against 50 mM Tris-HCl pH 7.4, 150 mM NaCl, 1 mM EDTA and 5% glycerol, snap-frozen in liquid N_2 and stored at -80 °C. Protein concentrations were determined with a NanoDrop spectrophotometer. Prior to use, protein solutions were ultra-centrifuged at 190,000 x g for 40 min to remove aggregated material. α-Synuclein (αSyn) was produced in *E. coli* BL21 (DE3) and monomeric αSyn was purified as described elsewhere (Theillet et al., 2016). Expression of Tau40 protein was performed in *E. coli* BL21 using a 50 l bioreactor. After cell disruption using a French press, Tau40 protein was purified via cation exchange chromatography and gel

filtration. Expression and purification of Tau were performed by InVivo BioTech Services (Hennigsdorf, Germany) using proprietary company protocols.

Preparation of *in vitro* seeds

Spontaneous Ex1Q48 aggregation was initiated by addition of 14 U PreScission protease (GE Healthcare) per nmol purified GST-Ex1Q48 fusion protein (2 µM). The aggregation reaction was performed in 50 mM Tris-HCl pH 7.4, 150 mM NaCl, 1 mM EDTA and 1 mM DTT at 25 °C and constant agitation (450 rpm) for 24 h. Ex1Q23 protein for seeding experiments was prepared from GST-Ex1Q23 fusion protein using the same protocol. Synthetic human IAPP was aggregated as described previously (Gao et al., 2015). Lyophilized αSyn was dissolved in PBS at 500 µM and centrifuged (4 °C, 265.000 x g) after a 5 min sonication step to remove aggregated material. The supernatant was incubated for 7 d at 37 °C under constant shaking in the presence of a single glass bead. Tau40 was aggregated for 6 d at 37 °C under constant shaking in 100 mM sodium acetate, pH 7.4, and 1 mM DTT in the presence of heparin. Synthetic human $A\beta_{1-42}$ was dissolved in 100 mM NaOH and diluted to 200 µM in low salt buffer (10 mM K_3PO_4, pH 7.4, 10 mM NaCl). Aggregation was performed for 6 h at 37 °C under constant agitation.

Atomic force microscopy

Aliquots of 15 µl aggregation reactions (24 h) were spotted onto freshly cleaved mica glued to a microscope slide. After incubation for 30 min to allow adsorption, samples were rinsed 4 times with 40 µl distilled water and dried over night at RT. Samples

were imaged with a digital multimode Nanowizard II (JPK, Germany) atomic force microscope operating in intermittent-contact mode.

Filter retardation assays

FRAs were essentially performed as described previously (Wanker et al., 1999). Briefly, equal volumes of 500 ng of Ex1Q48 aggregates and 4% SDS solution with 100 mM DTT were mixed and boiled at 95 °C for 5 min. By applying vacuum, samples were filtered through a cellulose acetate membrane with 0.2 µm pores (Schleicher and Schuell, Germany) and washed twice with 100 µl 0.1% SDS. For analysis of tissue homogenates, 60 µg of total protein for mouse brain and 75 µg of total protein for *Drosophila* heads were filtered per dot. Membranes were blocked with 5% skim milk in PBS/0.05% Tween20 (PBS-T) for at least 30 min. Aggregates retained on the membrane were detected using GFP, N18, MW8, Mab5492 or HD1 antibody followed by an appropriate peroxidase-coupled secondary antibody. Signals were quantified using the AIDA image analysis software (Raytest, Germany).

Dot blot assays

To estimate total HTT protein, native dot blot (DB) assays were performed as described previously (Kayed et al., 2003). Briefly, 250 ng of Ex1Q48 protein were filtered onto a nitrocellulose membrane and blocked with 5% skim milk in PBS-T. For detection, the membrane was incubated with HD1 antibody followed by an appropriate peroxidase-coupled secondary antibody. Signals were quantified using the AIDA image analysis software (Raytest, Germany).

Native gels

Protein solutions were mixed with sample buffer and loaded onto a Novex NativePAGE 3-12% Bis-Tris gradient gel (Life Technologies). NativePAGE and immunoblotting were performed according to manufacturer recommendations. Ex1Q48 aggregates were visualized as for SDS-PAGE.

SDS-PAGE and Western blotting

Samples of aggregation reactions were mixed with loading buffer (50 mM Tris-HCl pH 6.8, 2% SDS, 10% glycerol and 0.1% bromophenol blue) and boiled at 95 °C for 5 min. Samples were loaded onto Novex NuPAGE 4-12% Bis-Tris gradient gels (Life Technologies). SDS-PAGE and immunoblotting were performed according to manufacturer recommendations. Ex1Q48 distribution was visualized by N18 antibody (Santa Cruz) or Ex1Q48-CyPet/-YPet with a GFP antibody (Abcam) followed by appropriate peroxidase labeled secondary antibodies.

Genotyping of *Drosophila* strains

Total genomic DNA from transgenic flies was extracted using the DNeasy® Blood & Tissue Kit (Qiagen). cDNAs encoding HTTex1Q17 and HTTex1Q97 were PCR amplified using the Pwo DNA polymerase (Roche) and the primers 5'-aaccccgtaaatcaactgc- 3' and 5'-atctctgtaggtagtttgtc-3'). The sizes of the resulting PCR products were analyzed by agarose gel electrophoresis.

Quantitative polymerase chain reaction (qPCR)

RNA was extracted from *Drosophila* heads using TRIzol™ Reagent (Invitrogen). cDNA was synthesized using M-MLV Reverse Transcriptase (Thermo Scientific) and qPCR was performed using the SYBR Green PCR Master Mix (Thermo Scientific). Primer pairs for HTT (sense, 5′-gacctggaaaagctgatga-3′ and antisense 5′-tcatggtcggtgcagcggct-3′), and control primers for rp49 (sense 5′-tacaggcccaagatcgtgaa-3′, and antisense 5′-acgttgtgcaccaggaactt-3′) were utilized. SYBR Green analysis was performed using the ViiA7 Real-time PCR system (Thermo Scientific). The amount of mRNA detected was normalized to control rp49 mRNA values.

Viability analysis of adult *Drosophila melanogaster*

Viability assays were performed with elavGS;HTTex1Q17 and elavGS;HTTex1Q97 transgenic flies by quantification of lethality of at least 100 females of each genotype and expression condition in three independent biological replicates. Flies were aged at 25°C, with 10 flies per vial, and were transferred every 3-4 days. Median lifespan (age at which half of the tested population has died) was calculated by fitting survival curves to the log(inhibitor) vs. normalized response (variable slope) equation using GraphPad Prism. Statistical significance was assessed by one-way ANOVA followed by Dunnett's multiple comparison post hoc test. *, $p \leq 0.05$; **, $p \leq 0.01$; ***, $p \leq 0.001$.

Analysis of motor performance (climbing assay)

Ten female flies were placed in a closed empty vial and gently tapped to the bottom of the vial. The percentage of flies that climbed 8 cm within 15 s was recorded. Flies were aged at 25°C (10 flies per vial) and were monitored and transferred twice a week. Motor performance was assessed for elavGS;HTTex1Q17 and elavGS;HTTex1Q97 flies expressing the HTT transgenes for the indicated times. 100 females of each genotype and expression condition in each of the three biological replicates were investigated.

Preparation of *Drosophila* head lysates for FRAs

Drosophila head lysates were produced by homogenizing fly heads in 2 % SDS and complete protease inhibitor cocktail using a micro pestle. Lysates were centrifuged for 10 min at 8,000 rpm (4°C). The supernatant was transferred to a new tube and total protein concentration was determined with a Pierce™ BCA assay using BSA as a standard.

Dissection and immunostaining of *Drosophila* adult brain

The whole brain from adult flies were dissected in ice-cold haemolymph-like saline (HL3) solution (Steward et al., 1994), fixed for 20 min in 4 % paraformaldehyde (PFA) in PBS and permeabilized in PBS-T (1 % Triton™ X-100) for 20 min at RT. Samples were blocked in 10 % normal goat serum (NGS) in PBS-T (0.3 % Triton™ X-100) for at least two hours. Brains were incubated with the indicated primary antibody (1:500) in brain staining buffer (5 % NGS, 0.1 % NaN_3 in PBS-T (0.3 % Triton™ X-100)) for 48 hours at 4 °C. Subsequently, brains were washed in PBS-T (0.3 % Triton™ X-100) for 24 hours at 4°C with multiple buffer exchanges. Next, samples were incubated with appropriate secondary antibody in brain staining buffer for 24 hours at

4 °C, washed six times for 30 min in PBS-T (0.3 % Triton™ X-100) at RT and stored in VectaShield (H-100) (Vector Laboratories) at least for one day at -20 °C. Brains were mounted and imaged using the Leica TCS SP8 Confocal Microscope. Images were analyzed using Fiji.

RNA interference

For synchronization, gravid adults from one 10 cm NGM plate were collected in a canonical tube and treated with 20% alkaline hypochlorite solution under vigorous agitation for 4 min. The eggs were then washed three times with cold 0.1 M NaCl solution. The eggs were allowed to hatch in M9 medium at 20 °C for 22 h. Animals were then placed as L1 larvae onto RNAi plates that were seeded with *E. coli* expressing dsRNAi against *hsp-1* or the empty vector L4440 (control).

Fluorescence microscopy

The aggregation propensities of Q35-YFP were analyzed throughout adulthood. Animals were subjected to RNAi treatment from the first larval stage on and maintained on RNAi plates throughout the experiment. For imaging, nematodes were mounted onto 2% agarose (Sigma) pads on glass slides and immobilized with 2 mM Levamisole (Sigma). Images were taken on a Zeiss LSM780 confocal microscope at 20x magnification. The Q35-YFP expressing nematodes were analyzed as whole nematode for quantification of the aggregates and an image was taken of the head region of every animal. 20 animals were analyzed for each condition.

Motility assay

Nematodes were transferred from liquid culture onto a blank (unseeded) NGM plate and allowed to acclimate for 15 min. The movement of the animals was digitally recorded at 20 °C using a Leica M165FC microscope with a DFC3000G digital camera and the Leica LASX Software. Movies of 10 s were captured at 10 frames/s. Animals that crossed each other or those that escaped from the field of view were excluded from analysis. 20 animals were analyzed for each condition. Captured frames were merged into *.avi format, imported into Fiji (Schindelin et al., 2012) and analyzed using the wrMTrck plugin (http://www.phage.dk/plugins). The average speed of each animal was calculated by dividing its body length by the duration of each track (body length per second).

Tissue homogenization

Frozen brain tissue was cut on dry ice, weighed and homogenized in a 10-fold excess (w/v) of ice-cold 10 mM Tris-HCl pH 7.4, 0.8 M NaCl, 1 mM EDTA, 10% sucrose, 0.25 U/µl benzonase and complete protease inhibitor cocktail with a dounce homogenizer. The homogenate was incubated for 1 h at 4 °C on a rotating wheel and centrifuged for 20 min at 2,700 x g (4 °C) to remove cell debris. *Drosophila* heads were processed comparably using 10 µl of ice-cold 10 mM Tris-HCl pH 7.4, 0.8 M NaCl, 1 mM EDTA, 10% sucrose and a complete protease inhibitor cocktail per fly head. Homogenates were centrifuged for 10 min at 8,000 rpm (4°C). After centrifugation, supernatants were transferred to a new tube and total protein concentration was determined with a Pierce™ BCA assay using BSA as a standard. For FRASE analysis, 0.8-5 µg total protein per replicate were applied.

Electron microscopy

Total brain homogenate was centrifuged at 18,000 x g at 4 °C for 20 min; the resulting supernatant was pelleted by ultra-centrifugation at 190,000 x g for 40 min and resuspended in 10 mM Tris-HCl (pH 7.4). Immunolabeling was performed with minor modifications as described (Laue, 2010). Briefly, samples were incubated on formvar-coated copper grids (Plano) for 10 min before immunolabeling. Grids were blocked and washed in PBS supplemented with 1% BSA and 0.1% glycine. Labeling was performed with the anti-HTT aggregate antibody AGG and an appropriate 12 nm colloidal gold-labeled secondary antibody (Jackson ImmunoResearch). Samples were stained with 2% uranyl acetate and imaged with a Zeiss EM 910 transmission electron microscope at 80 kV. Acquisition was performed with a CDD camera (Quemesa, Olympus Viewing System); pictures were processed using Adobe Illustrator.

Immunodepletion of HTT aggregates from mouse brain extracts

Protein G-coupled magnetic beads (Life Technologies) were incubated with 4 µg MW8 (Developmental Studies Hybridoma Bank, DSHB) or IgG isotype control (Invitrogen) antibody, respectively, for 10 min at RT to allow antibody binding. Free binding sites were saturated with Pierce protein-free blocking solution according to manufacturer recommendations. 500 µg brain homogenate in brain lysis buffer were incubated with antibody coupled beads for 3 h at 4 °C under constant overhead rotation. Subsequently, aliquots from the supernatants were taken and analyzed with the FRASE assay.

FRASE assay

Purified GST-Ex1Q48-CyPet and GST-Ex1Q48-YPet were diluted in aggregation buffer at an equimolar ratio to a final concentration of 1.2 µM (0.6 µM each) with 14 U PSP per nmol sensor proteins if not stated otherwise. The solution was then mixed with preformed aggregates of Ex1Q48 (seeds) at varying concentrations with or without prior sonication and transferred to a black 384-well plate (with a final reaction volume of 30 µl per well and a sensor protein concentration of 1.2 µM). For quantification of seeding-competent HTT species in tissue samples, the sensor-protein mixture was supplemented with up to 10% (v/v) tissue homogenate. Fluorescence signals were measured every 20 min following a 5 s pulse of vertical shaking with a Tecan M200 fluorescence plate reader at 25 °C for up to 48 h. CyPet donor fluorescence was measured at excitation (Ex): 435 nm/emission (Em): 475 nm; YPet acceptor fluorescence at Ex: 500 nm/Em: 530 nm; the FRET channel (DA) was recorded at Ex: 435 nm/Em: 530 nm. Raw signals were processed by subtracting the background fluorescence of unlabeled Ex1Q48 in all channels. Signals in the FRET channel were corrected for donor bleed-through (c_D) and acceptor cross excitation (c_A) using donor- and acceptor-only samples to obtain sensitized emission. Finally, sensitized emission was normalized to the acceptor signals (Jiang and Sorkin, 2002). In brief, the FRET efficiency E (in %) was calculated as follows: $E = (DA-c_D x DD-c_A x AA)/AA$ with DD = donor channel signal and AA = acceptor channel signal.

Quantification of mutant HTT seeding activity (HSA)

Seeding effects (Δt_{50} [h]) were quantified by subtracting the t_{50} values (time at half-maximal FRET efficiency) of the respective sample from the negative control. To obtain the t_{50} values, the aggregation kinetics were curve fitted by Richard's five-parameter dose-response curve using GraphPad Prism.

$$y = y_0 + \left(\frac{y_\infty - y_0}{1 + 10^{((Logxb - x) \times HillSlope)^S}}\right)$$

QUANTIFICATION AND STATISTICAL ANALYSIS

Statistical parameters including the exact value of n, the definition of center, dispersion and precision measures (mean ± SEM or mean ± SD) as well as the statistical analysis chosen and statistical significance are reported in the Figures and Figure Legends. Data is judged to be statistically significant when $p < 0.05$ by the indicated statistical test. In figures, asterisks denote statistical significance as calculated by Student's t test (*, $p < 0.05$; **, $p < 0.01$; ***, $p < 0.001$). Statistical analysis was performed in GraphPad PRISM 7.

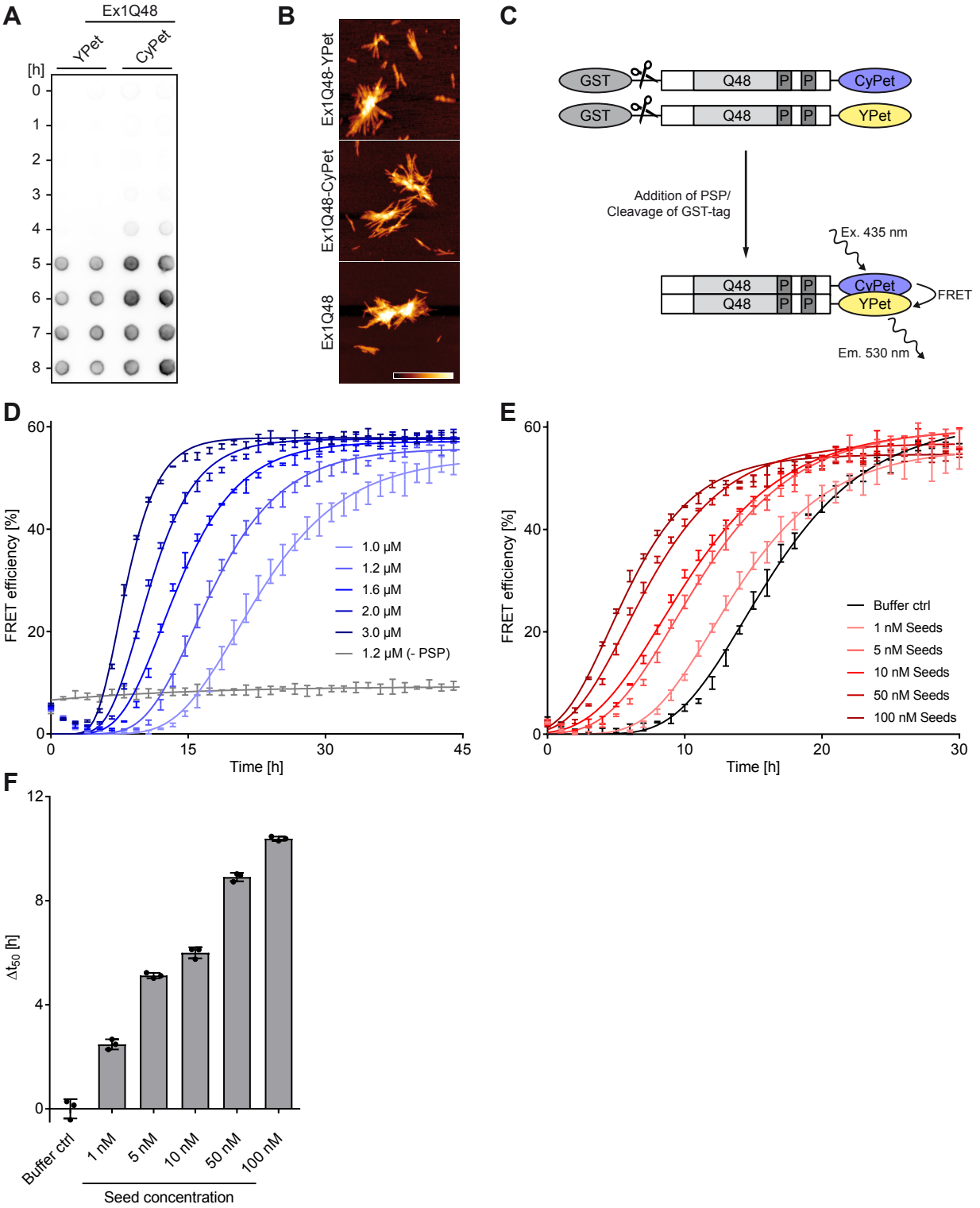
A
Ex1Q48
YPet
CyPet
[h]
0
1
2
3
4
5
6
7
8
B
Ex1Q48-YPet
Ex1Q48-CyPet
Ex1Q48
C
GST
Q48
P
P
CyPet
YPet
Addition of PSP/
Cleavage of GST-tag
Ex. 435 nm
FRET
Em. 530 nm
D
FRET efficiency [%]
Time [h]
1.0 µM
1.2 µM
1.6 µM
2.0 µM
3.0 µM
1.2 µM (- PSP)
E
FRET efficiency [%]
Time [h]
Buffer ctrl
1 nM Seeds
5 nM Seeds
10 nM Seeds
50 nM Seeds
100 nM Seeds
F
Δt50 [h]
Buffer ctrl
1 nM
5 nM
10 nM
50 nM
100 nM
Seed concentration

Figure 1

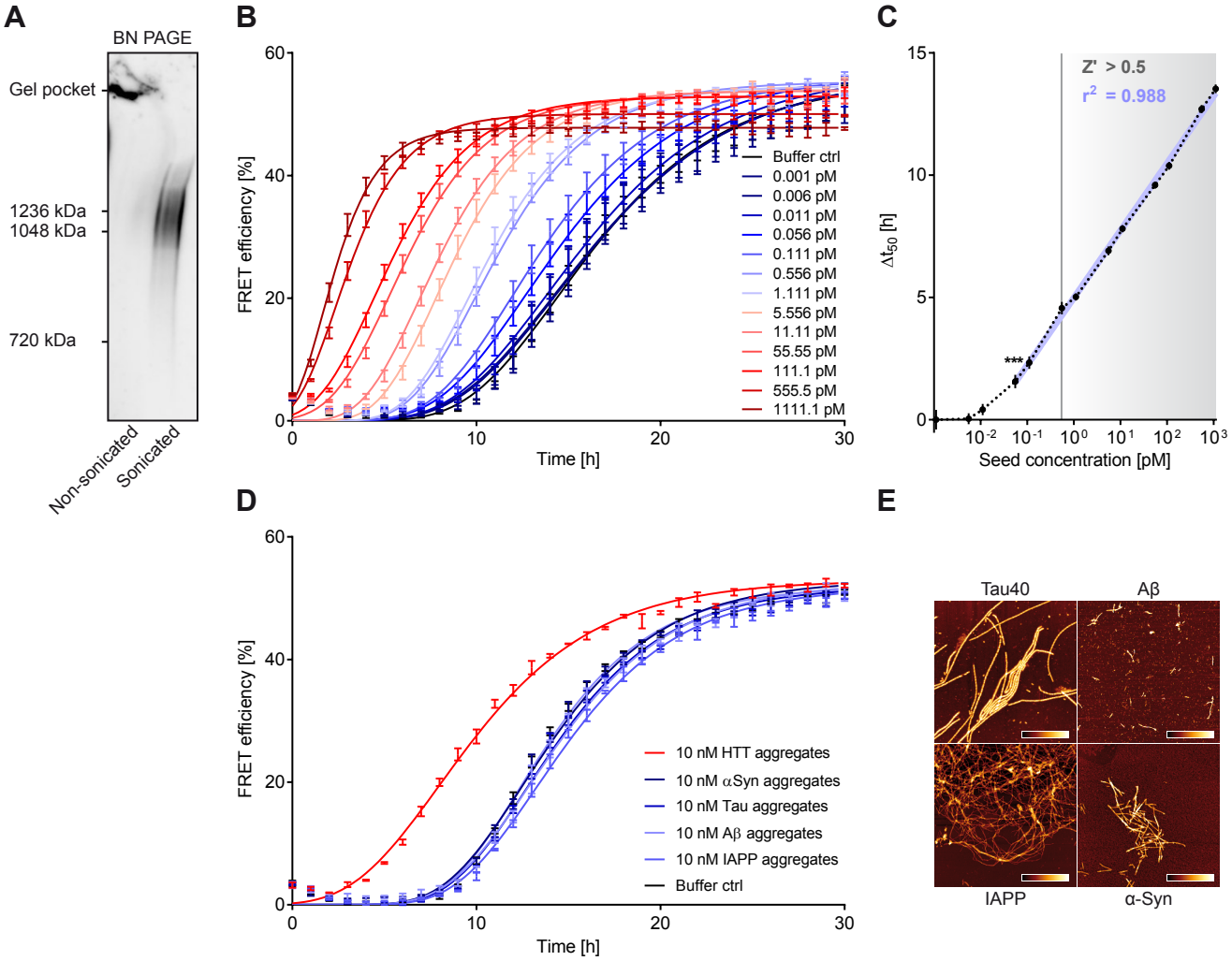
A
BN PAGE
Gel pocket
1236 kDa
1048 kDa
720 kDa
Non-sonicated
Sonicated
B
FRET efficiency [%]
Time [h]
Buffer ctrl
0.001 pM
0.006 pM
0.011 pM
0.056 pM
0.111 pM
0.556 pM
1.111 pM
5.556 pM
11.11 pM
55.55 pM
111.1 pM
555.5 pM
1111.1 pM
C
Z' > 0.5
r² = 0.988
Δt50 [h]
Seed concentration [pM]
***
D
FRET efficiency [%]
Time [h]
10 nM HTT aggregates
10 nM αSyn aggregates
10 nM Tau aggregates
10 nM Aβ aggregates
10 nM IAPP aggregates
Buffer ctrl
E
Tau40
Aβ
IAPP
α-Syn

Figure 2

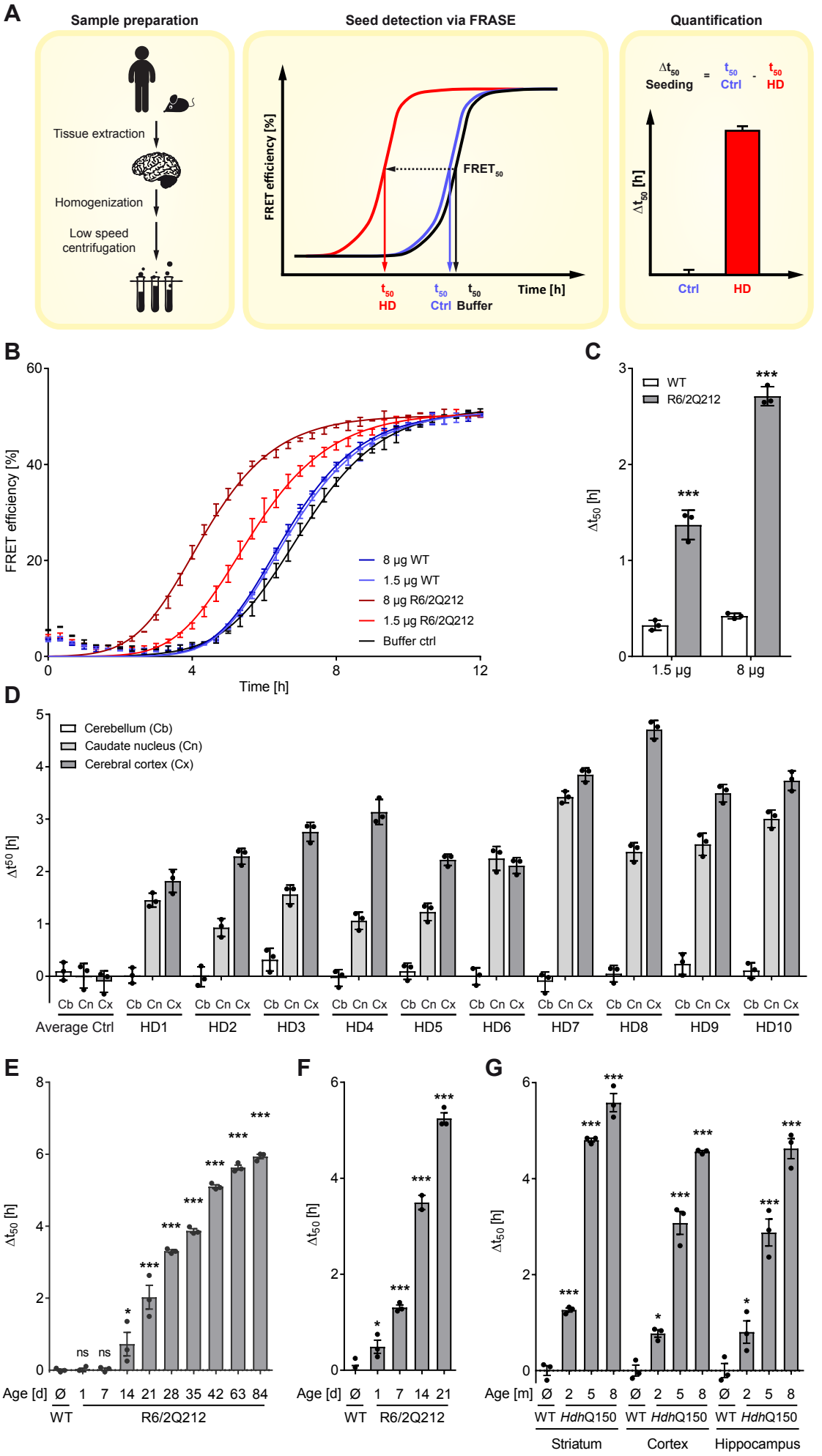
A
Sample preparation
Tissue extraction
Homogenization
Low speed centrifugation
Seed detection via FRASE
FRET efficiency [%]
FRET50
t50 HD
t50 Ctrl
t50 Buffer
Time [h]
Quantification
Δt50 Seeding = t50 Ctrl - t50 HD
Δt50 [h]
Ctrl
HD
B
FRET efficiency [%]
Time [h]
8 µg WT
1.5 µg WT
8 µg R6/2Q212
1.5 µg R6/2Q212
Buffer ctrl
C
WT
R6/2Q212
Δt50 [h]
1.5 µg
8 µg
D
Cerebellum (Cb)
Caudate nucleus (Cn)
Cerebral cortex (Cx)
Δt50 [h]
Average Ctrl
HD1
HD2
HD3
HD4
HD5
HD6
HD7
HD8
HD9
HD10
E
Δt50 [h]
Age [d] Ø 1 7 14 21 28 35 42 63 84
WT
R6/2Q212
F
Δt50 [h]
Age [d] Ø 1 7 14 21
WT
R6/2Q212
G
Δt50 [h]
Age [m] Ø 2 5 8 Ø 2 5 8 Ø 2 5 8
WT HdhQ150 WT HdhQ150 WT HdhQ150
Striatum
Cortex
Hippocampus

Figure 3

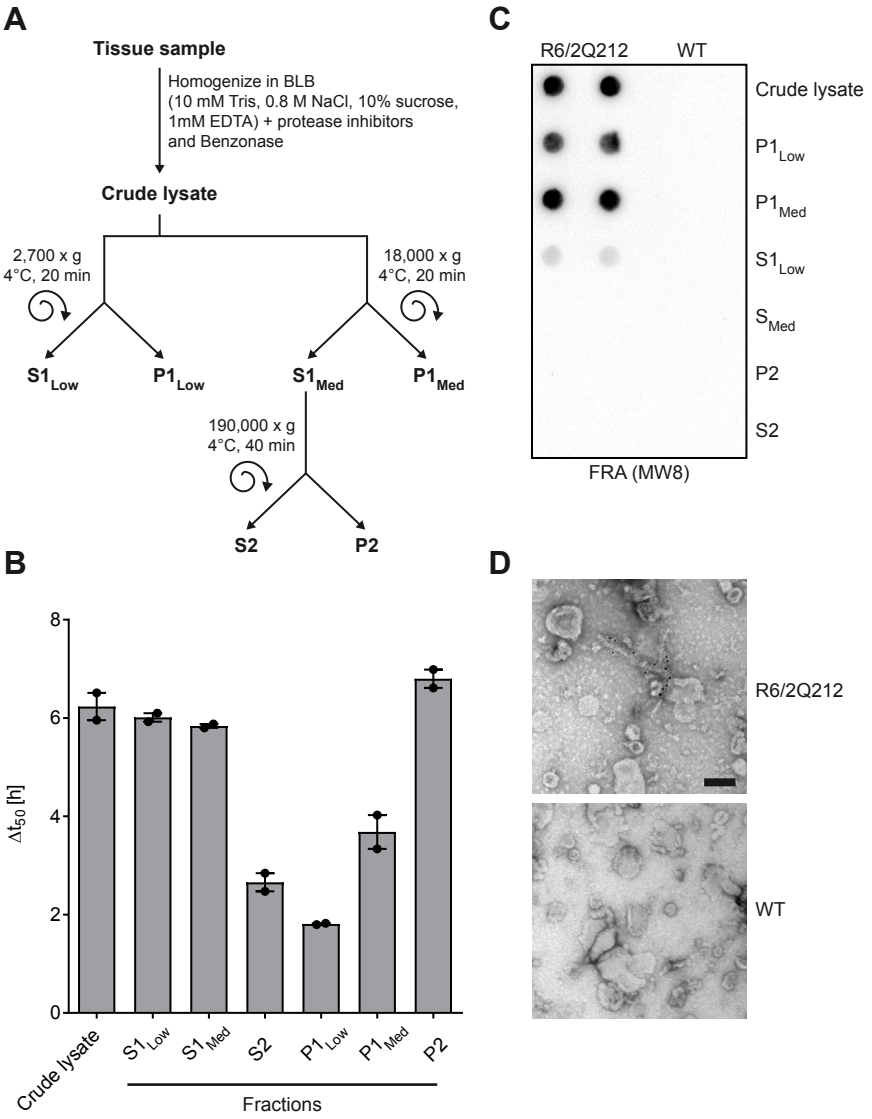
A
Tissue sample
Homogenize in BLB
(10 mM Tris, 0.8 M NaCl, 10% sucrose,
1mM EDTA) + protease inhibitors
and Benzonase
Crude lysate
2,700 x g
4°C, 20 min
18,000 x g
4°C, 20 min
S1Low
P1Low
S1Med
P1Med
190,000 x g
4°C, 40 min
S2
P2
B
Δt50 [h]
Crude lysate
S1Low
S1Med
S2
P1Low
P1Med
P2
Fractions
C
R6/2Q212
WT
Crude lysate
P1Low
P1Med
S1Low
SMed
P2
S2
FRA (MW8)
D
R6/2Q212
WT

Figure 4

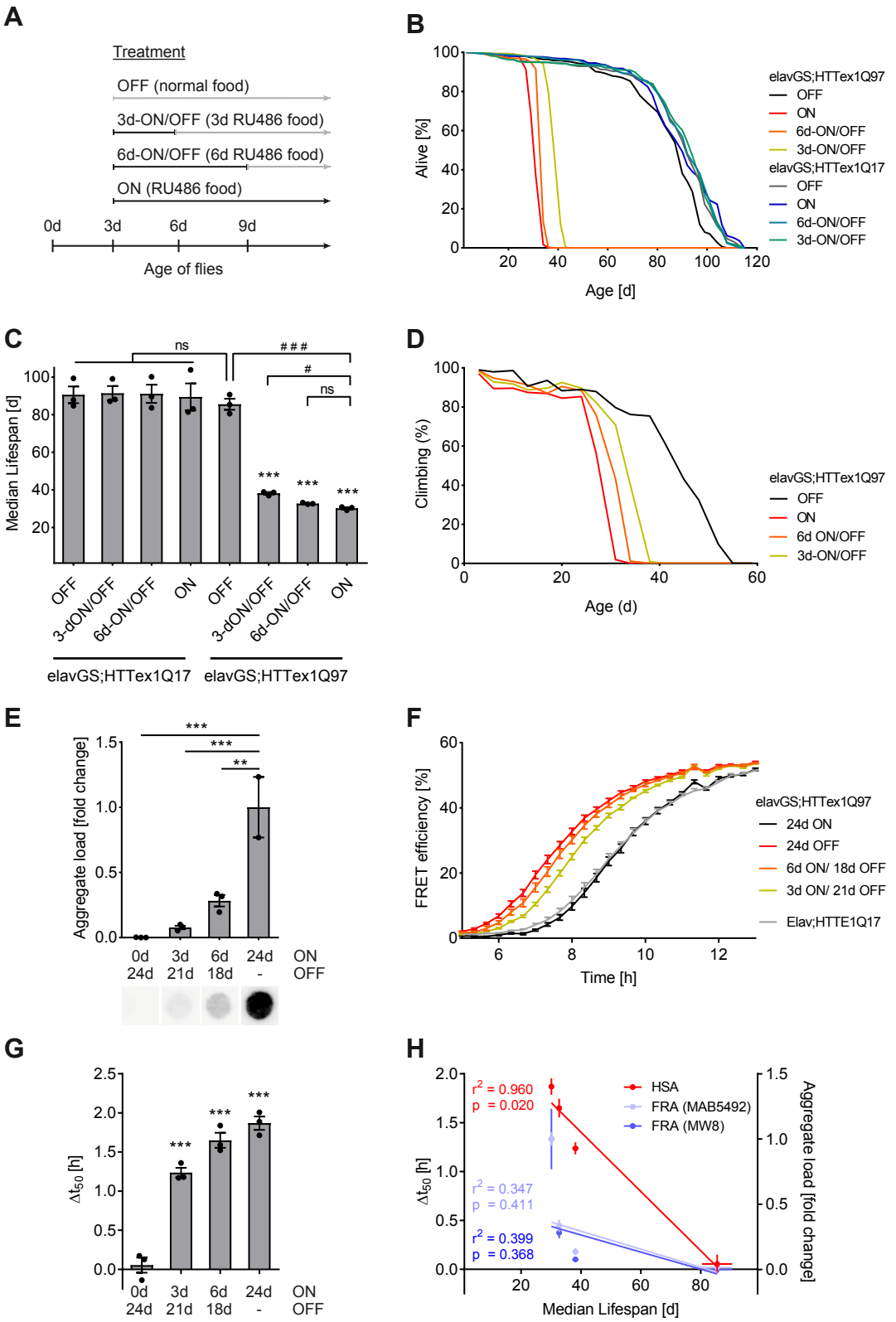
A
Treatment
OFF (normal food)
3d-ON/OFF (3d RU486 food)
6d-ON/OFF (6d RU486 food)
ON (RU486 food)
0d
3d
6d
9d
Age of flies
B
Alive [%]
Age [d]
elavGS;HTTex1Q97
OFF
ON
6d-ON/OFF
3d-ON/OFF
elavGS;HTTex1Q17
OFF
ON
6d-ON/OFF
3d-ON/OFF
C
Median Lifespan [d]
ns
###
#
ns
***
***
***
OFF
3-dON/OFF
6d-ON/OFF
ON
OFF
3-dON/OFF
6d-ON/OFF
ON
elavGS;HTTex1Q17
elavGS;HTTex1Q97
D
Climbing (%)
Age (d)
elavGS;HTTex1Q97
OFF
ON
6d ON/OFF
3d-ON/OFF
E
Aggregate load [fold change]
***
***
**
0d 24d
3d 21d
6d 18d
24d -
ON
OFF
F
FRET efficiency [%]
Time [h]
elavGS;HTTex1Q97
24d ON
24d OFF
6d ON/ 18d OFF
3d ON/ 21d OFF
Elav;HTTE1Q17
G
Δt50 [h]
***
***
***
0d 24d
3d 21d
6d 18d
24d -
ON
OFF
H
r2 = 0.960
p = 0.020
r2 = 0.347
p = 0.411
r2 = 0.399
p = 0.368
HSA
FRA (MAB5492)
FRA (MW8)
Δt50 [h]
Aggregate load [fold change]
Median Lifespan [d]

Figure 5

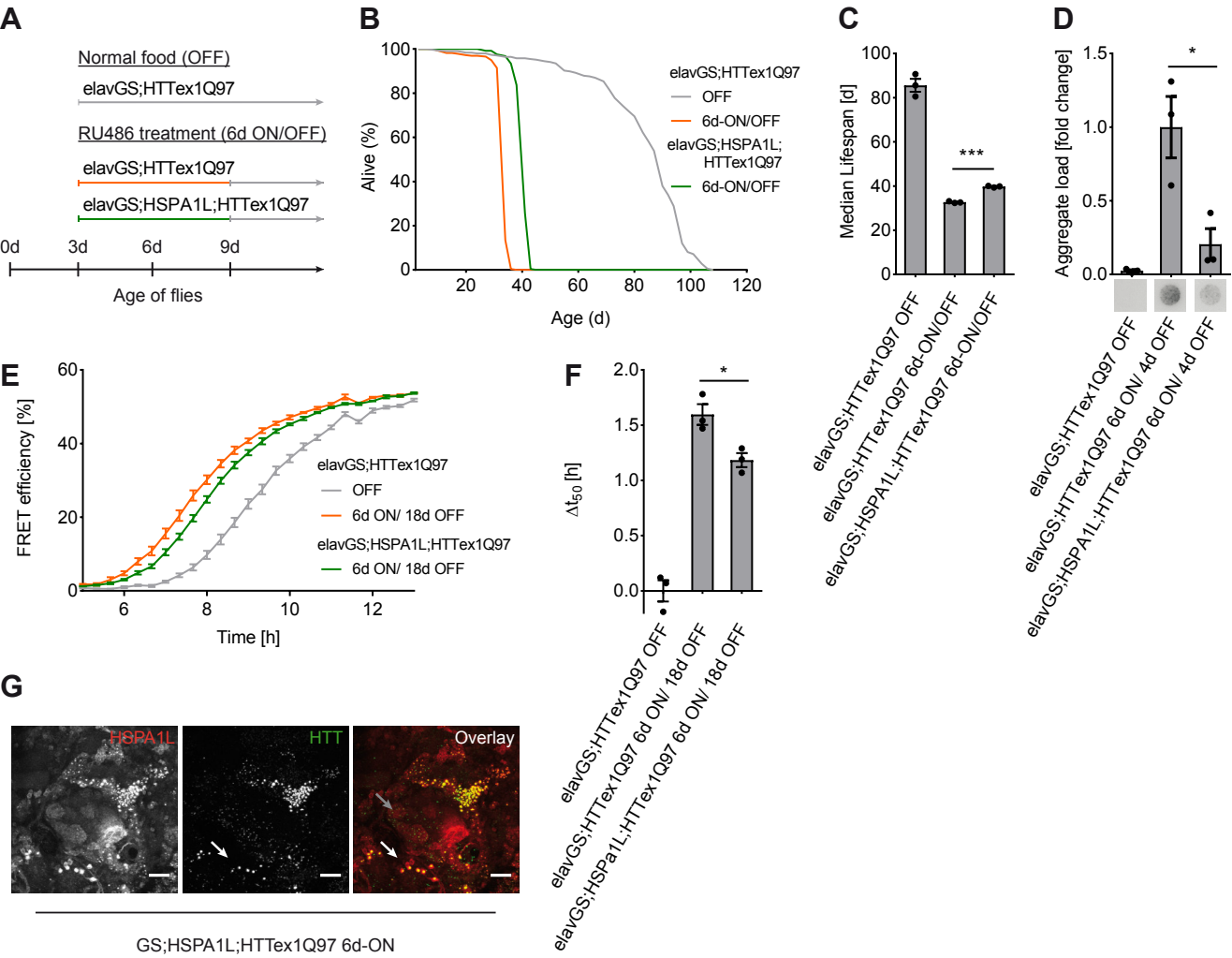
A
Normal food (OFF)
elavGS;HTTex1Q97
RU486 treatment (6d ON/OFF)
elavGS;HTTex1Q97
elavGS;HSPA1L;HTTex1Q97
0d
3d
6d
9d
Age of flies
B
Alive (%)
Age (d)
elavGS;HTTex1Q97
OFF
6d-ON/OFF
elavGS;HSPA1L;
HTTex1Q97
6d-ON/OFF
C
Median Lifespan [d]
***
elavGS;HTTex1Q97 OFF
elavGS;HTTex1Q97 6d-ON/OFF
elavGS;HSPA1L;HTTex1Q97 6d-ON/OFF
D
Aggregate load [fold change]
*
elavGS;HTTex1Q97 OFF
elavGS;HTTex1Q97 6d ON/ 4d OFF
elavGS;HSPA1L;HTTex1Q97 6d ON/ 4d OFF
E
FRET efficiency [%]
Time [h]
elavGS;HTTex1Q97
OFF
6d ON/ 18d OFF
elavGS;HSPA1L;HTTex1Q97
6d ON/ 18d OFF
F
Δt50 [h]
*
elavGS;HTTex1Q97 OFF
elavGS;HTTex1Q97 6d ON/ 18d OFF
elavGS;HSPa1L;HTTex1Q97 6d ON/ 18d OFF
G
HSPA1L
HTT
Overlay
GS;HSPA1L;HTTex1Q97 6d-ON

Figure 6

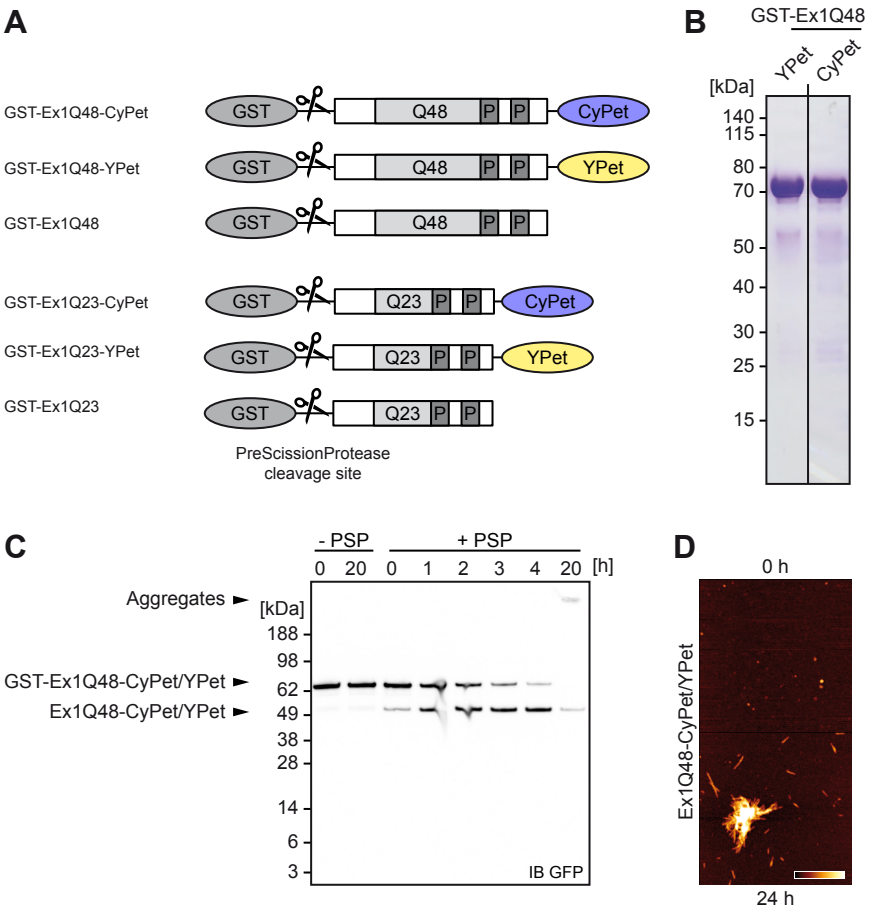

Supplementary Figure 1

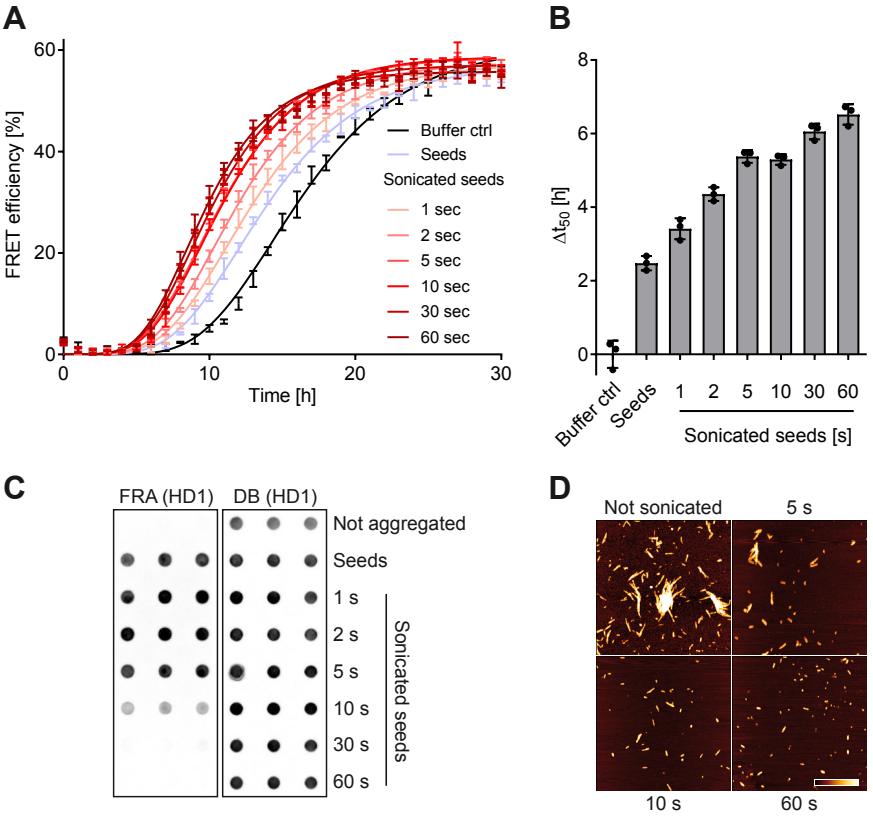

Supplementary Figure 2

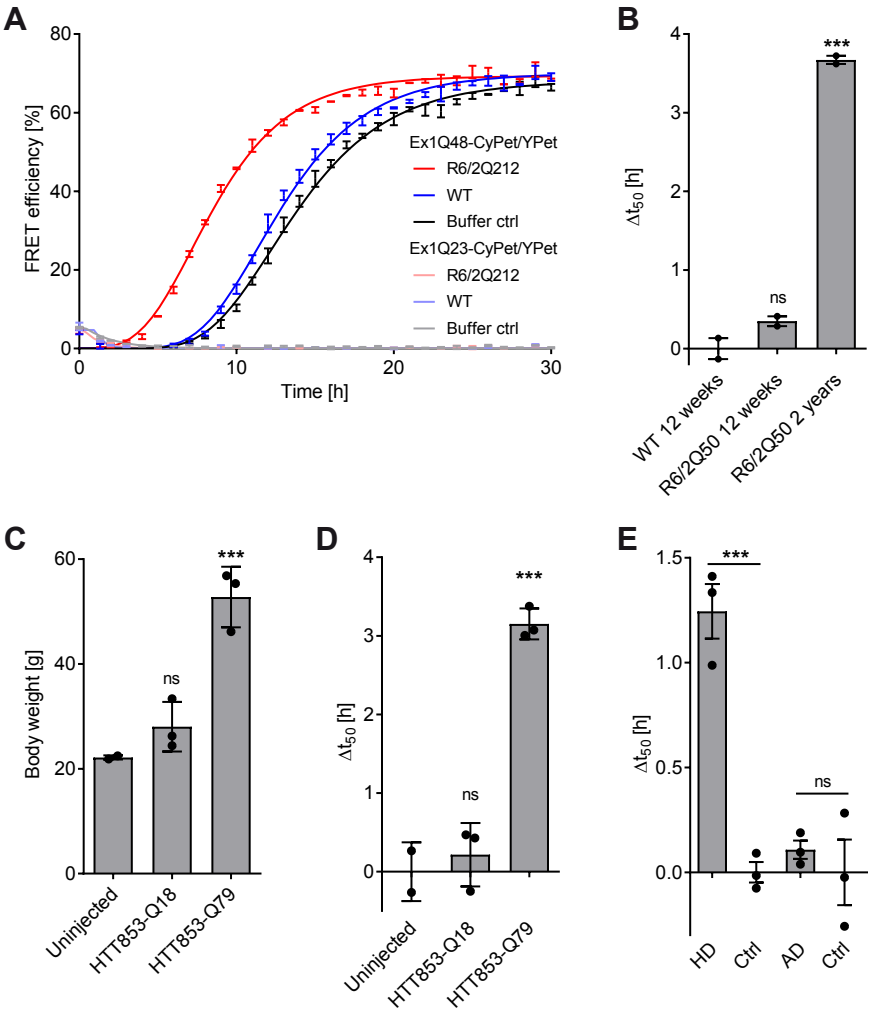

Supplementary Figure 3

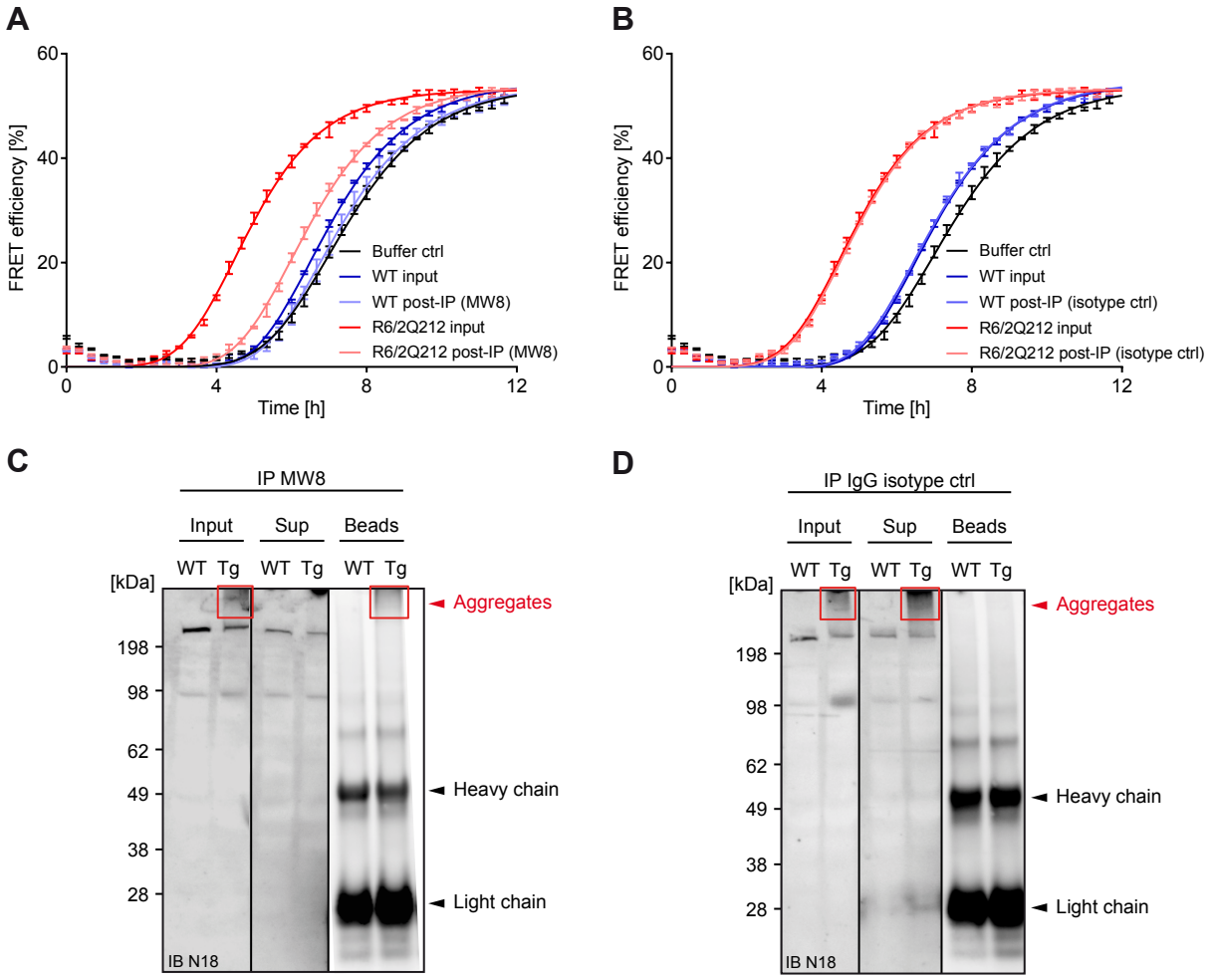

Supplementary Figure 4

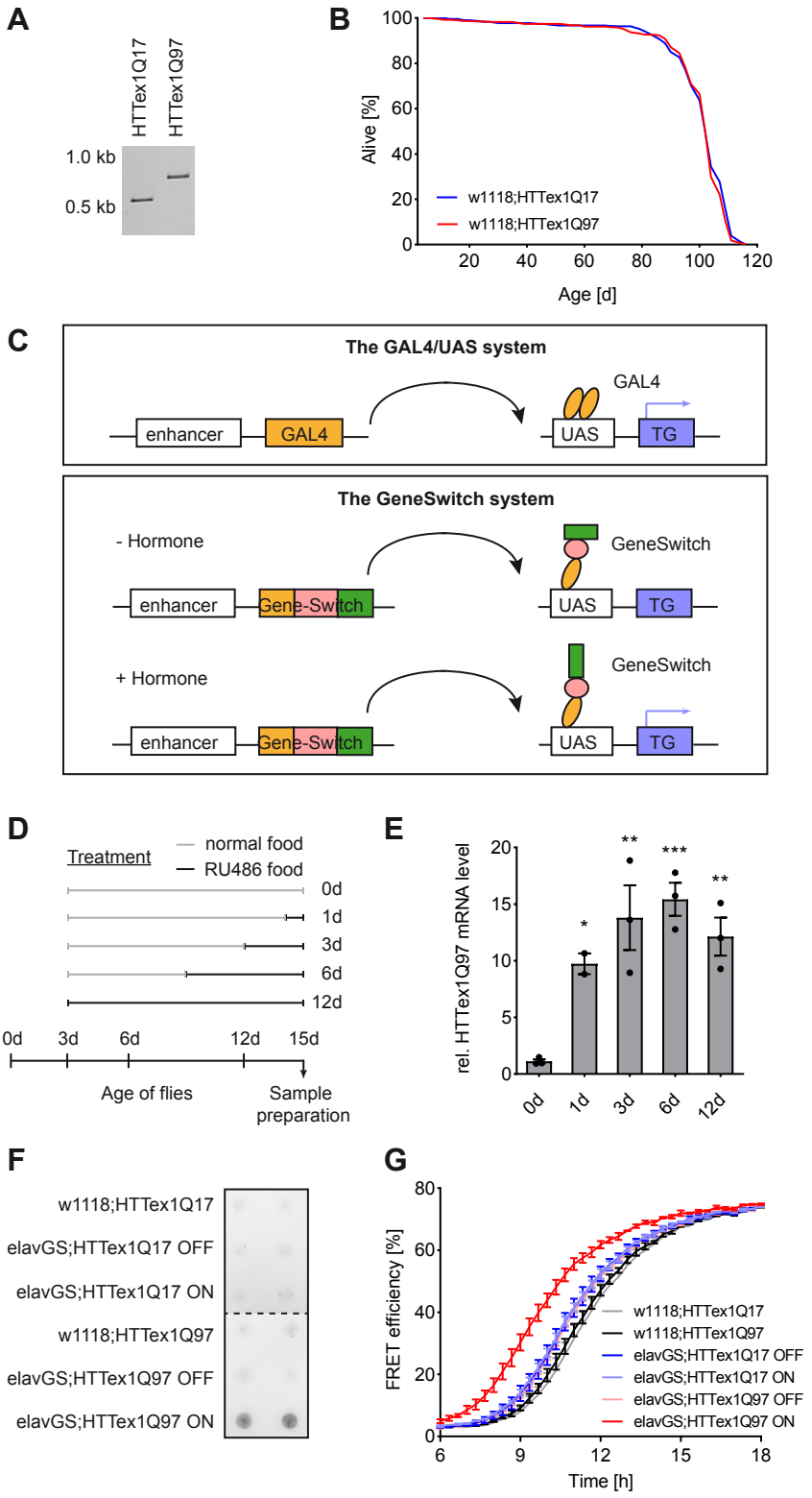

Supplementary Figure 5

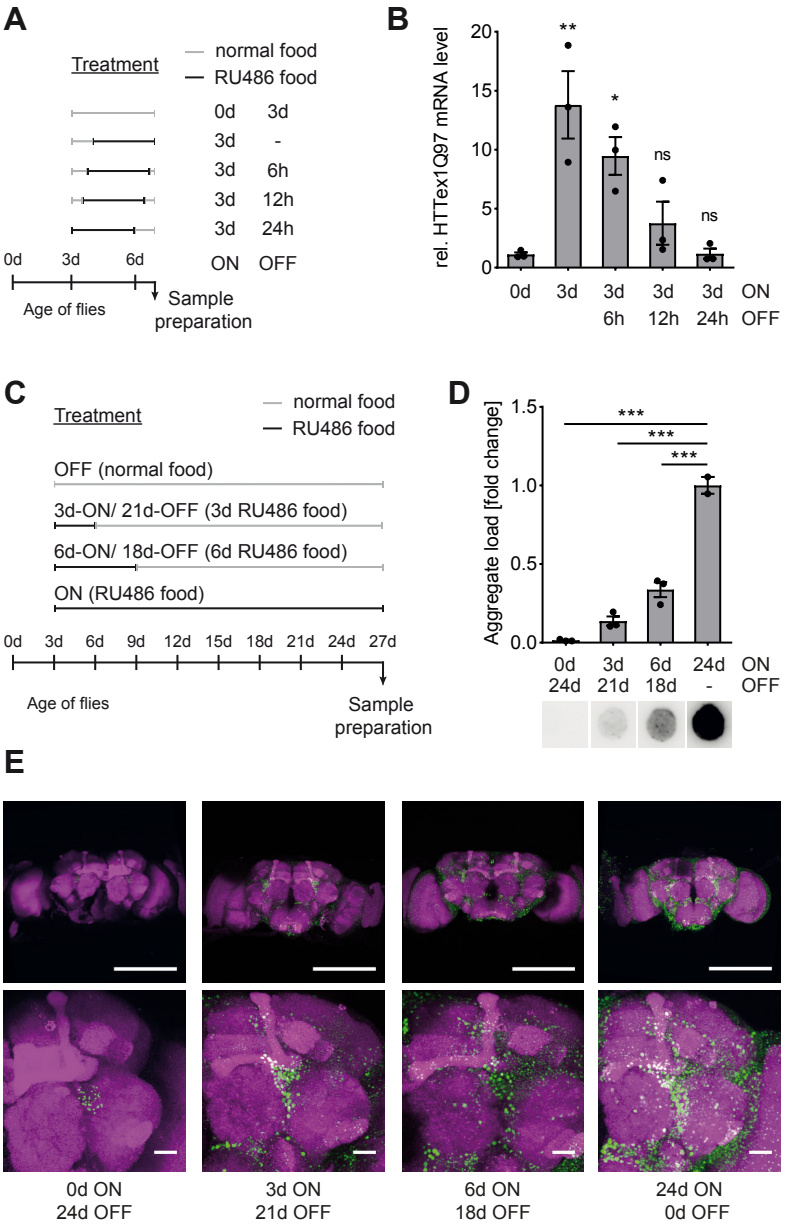

Supplementary Figure 6

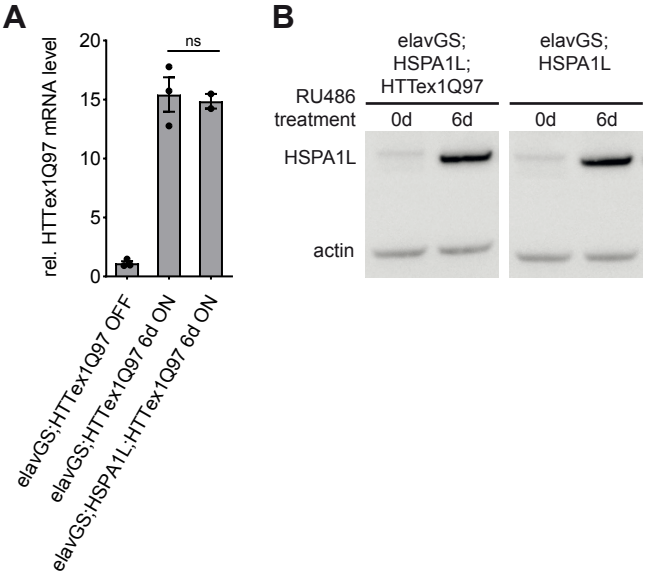

Supplementary Figure 7

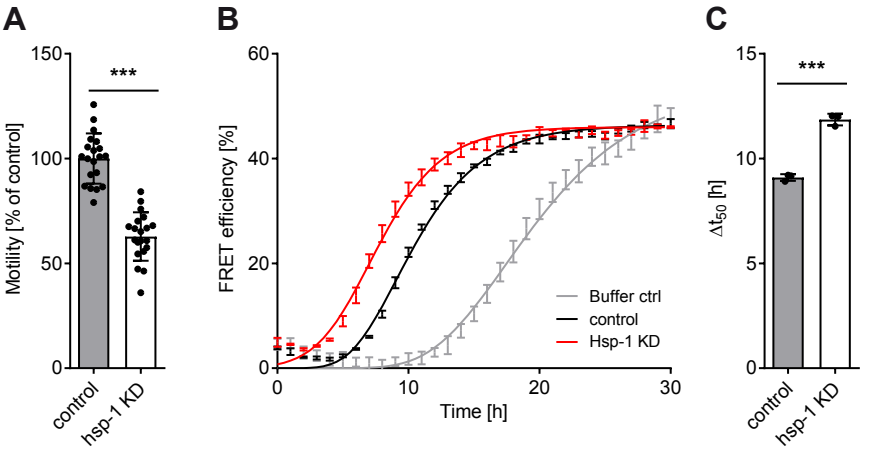

Supplementary Figure 8